# Restructuring of genomic provinces of surface ocean plankton under climate change

Paul Frémont, Marion Gehlen, Mathieu Vrac, Jade Leconte, Tom O. Delmont, Patrick Wincker, Daniele Iudicone, Olivier Jaillon

# Restructuring of genomic provinces of surface ocean plankton under climate change

Paul Frémont[1,2*], Marion Gehlen[3*], Mathieu Vrac[3], Jade Leconte[1,2], Tom O. Delmont[1,2], Patrick Wincker[1,2], Daniele Iudicone[4], Olivier Jaillon[1,2*]

[1]Génomique Métabolique, Genoscope, Institut François Jacob, CEA, CNRS, Université d'Evry, Université Paris-Saclay, 91057 Evry, France. [2]Research Federation for the study of Global Ocean Systems Ecology and Evolution, FR2022/Tara Oceans, Paris, France. [3]LSCE-IPSL, CEA/CNRS/Université Paris-Saclay, Gif-sur-Yvette, France. [4]Stazione Zoologica Anton Dhorn. Villa Comunale, 80121, Naples, Italy.

*Corresponding authors: pfremont@genoscope.cns.fr; marion.gehlen@lsce.ipsl.fr; ojaillon@genoscope.cns.fr

**The impact of climate change on diversity, functioning and biogeography of marine plankton is a major unresolved issue. Here, niche theory is applied to plankton metagenomes of 6 size fractions, from viruses to meso-zooplankton, sampled during the *Tara* Oceans expedition. Niches are used to derive plankton size-dependent structuring of the oceans south of 60°N in *climato-genomic* provinces characterized by signature genomes. By 2090, assuming the RCP8.5 high warming scenario, provinces would be reorganized over half of the considered oceans and quasi-systematically displaced poleward. Particularly, tropical provinces would expand at the expense of temperate ones. Compositional shifts among planktonic grazers and nitrogen-fixing bacteria suggest impacts on the nitrogen and carbon cycles. Sea surface temperature is identified as the main driver of the changes (~51%) followed by phosphate (11%) and salinity (10%). These results demonstrate the potential of integration of genomics with physico-chemical data for higher scale modeling and understanding of ocean ecosystem dynamics.**

Planktonic communities are composed of complex and heterogeneous assemblages of small animals, single-celled eukaryotes (protists), bacteria, archaea and viruses - that drift with currents. They contribute to the regulation of the Earth system through primary production via photosynthesis[1], carbon export to the deep oceans[2,3] and form the base of the food webs that sustain the whole trophic chain in the oceans and beyond[4].

The composition of communities varies over time at a given site with daily[5] to seasonal fluctuations[6] following environmental variability[7]. Overlying these relatively short scale

spatio-temporal variations, a more macroscale partitioning of the ocean has been revealed by different combinations of biological and physico-chemical data[8–10], and recently documented at the resolution of community genomics[11]. The basin scale biogeographical structure has been proposed to result from a combination of multiple bio-physico-chemical processes named the seascape[7]. These processes include both abiotic and biotic interactions[12], neutral genetic drift[13], natural selection[14,15], temperature variations, nutrient supply but also advection and mixing along currents[11,13].

Today, knowledge of global scale plankton biogeography at the DNA level is in its infancy. We lack understanding and theoretical explanations for the emergence and maintenance of biogeographical patterns at genomic resolution. Omics data (*i.e.* the DNA/RNA sequences representative of the variety of coding and non-coding sequences of organisms) provide the appropriate resolution to track and record global biogeographical features[11], modulation of the repertoire of expressed genes in a community in response to environmental conditions[2,16,17] and eco-evolutionary processes[13–15]. Moreover, metagenomic sequencing can be consistently analyzed across plankton organisms as recently demonstrated by global expeditions[18–21]. The strong links between plankton and environmental conditions suggest potentially major consequences of climate change on community composition and biogeography[22,23]. Time series observations have highlighted recent changes in the planktonic ecosystem attributed to anthropogenic pressures, such as changes in community composition[24,25] or poleward shifts of some species[26]. These changes are expected to intensify with ongoing climate warming[27] and could lead to major reorganization of plankton community composition[22], with a potential decline in diversity[28–30]. Another major consequence of global reorganization of the seascape on biological systems would be a decrease of primary production at mid-latitudes and an increase at higher latitudes[27].

Here we report the global structure of plankton biogeography south of 60°N based on metagenomic data using niche models and its putative modifications under climate change. First, we define environmental niches[31], *i.e.* the envelope of environmental parameters suitable for an organism or a population, at the scale of genomic provinces across 6 organism size fractions representing major plankton groups from nano- (viruses) to meso-zooplankton (small metazoans). Then, we spatially extrapolate their

niches into *climato-genomic* provinces to derive the structure of plankton biogeography for each size fraction individually and for all combined. Next, considering the same niches, we assess the spatial reorganization of these provinces under climate change at the end of the century, with a focus on associated compositional shifts among copepods (planktonic grazers important for the carbon cycle) and nitrogen-fixing bacteria (important for both nitrogen and carbon cycles). Finally, we quantify the relative importance of the environmental drivers explaining projected changes.

**Niche models and signature genomes from genomic provinces**

We define and validate environmental niches using 4 machine learning techniques for 27 previously defined genomic provinces[11]; they correspond to 529 metagenomes for 6 size fractions (ranging from 0 to 2000 µm) sampled at 95 sites from all oceans except the Arctic (Supplementary information 1, Supplementary Figs. 1-2). Predictor variables of the niches are sea surface temperature (SST), salinity, dissolved silica, nitrate, phosphate and iron, plus a seasonality index of nitrate.

The signal of ocean partitioning is likely due to abundant and compact genomes whose geographical distributions closely match provinces. Within a collection of 1778 bacterial, 110 archaeal and 713 eukaryotic environmental genomes[32,33] characterized from *Tara* Oceans samples without cultivation, we find a total of 324 signature genomes covering all but 4 provinces, and displaying taxonomic signal coherent with the size fractions (Fig. 1 for eukaryotes and Supplementary Fig. 3 for Bacteria and Archaea). Some of the signature genomes correspond to unexplored lineages with no cultured representatives, highlighting the knowledge gap for organisms that structure plankton biogeography and the strength of a rationale devoid of any *a priori* on reference genomes or species.

**Structure of present day biogeography of plankton**

To extrapolate the niches to a global ocean biogeography for each size fraction, we define the most probable provinces, named hereafter as *dominant* and assigned to a climatic annotation (Supplementary Table 1), on each 1°x1° resolution grid point using 2006-13 WOA13 climatology[34] (Supplementary Fig. 4 and Fig. 2).

In agreement with previous observations[11], provinces of large size fractions (>20 µm) are wider and partially decoupled from those of smaller size fractions, probably due to differential responses to oceanic circulation and environmental variations, different life

cycle constraints, lifestyles[7,11] and trophic network positions[35]. Biogeographies of small metazoans that enrich the largest size fractions (180-2000 and 20-180 µm) are broadly aligned with latitudinal bands (tropico-equatorial, temperate and (sub)-polar) dominated by a single province (Fig. 2ab). A more complex oceanic structuring emerges for the smaller size fractions (<20 µm) (Fig. 2c-f) with several provinces per large geographical region. For size fraction 0.8-5 µm enriched in small protists (Fig. 2d), distinct provinces are identified for tropical oligotrophic gyres and for the nutrient-rich equatorial upwelling region. A complex pattern of provinces, mostly latitudinal, is found for the bacteria (Fig. 2e, 0.22-3 µm) and the virus enriched size classes (Fig. 2f, 0-0.2 µm) although less clearly linked to large-scale oceanographic regions. A single province extending from temperate to polar regions emerges for size fraction 5-20 µm enriched in protists (Fig. 2c), for which fewer samples were available (Supplementary Fig. 2b-c), which probably biases this result. A consensus map combining all size fractions, built using the PHATE algorithm[36], summarizes the main characteristics of the biogeographies described above (Supplementary information 2 and Supplementary Fig. 5).

Finally, we compare genomic biogeographies and existing ocean partitionings[8–10]. Though each of them is unique (Supplementary Fig. 8-10), common borders highlight a global latitudinal partitioning independent of the type of data (Supplementary information 3).

**Future changes in plankton biogeography structure**

We assess the impacts of climate change on plankton biogeography at the end of the century following the Representative Concentration Pathway 8.5 (RCP8.5)[37] greenhouse gas concentration trajectory. To consistently compare projections of present and future biogeographies, we use bias-adjusted mean of 6 Earth System Model (ESM) climatologies (Supplementary Table 2, Supplementary Fig. 11). The highest warming (7.2°C) is located off the east coast of Canada in the North Atlantic while complex patterns of salinity and nutrient variations are projected in all oceans (Supplementary Fig. 12). Following this trajectory, future temperature at most sampling sites will be higher than the mean and maximum contemporary temperature within their current province (Supplementary Fig. 13).

Our projections indicate multiple large-scale changes in biogeographical structure including expansions, shrinkages and shifts in plankton organism size-dependent provinces (Fig. 2a-d, Supplementary Fig. 14-16). A change in the *dominant* province in at least one size fraction would occur over 60.1% of the ocean surface, ranging from 12% (20-180 µm) to 31% (0.8-5 µm) (Fig. 2, Table 1).

Centroids of provinces with *dominance* areas larger than $10^6$ $km^2$ within a basin would be moved at least 200 km away for 77% of them, 96% of which move poleward (Supplementary Figs. 15 and 16). While a few longitudinal shifts larger than 1000 km are projected, the distribution of latitudinal shifts is largely concentrated around the mean (290 km) with no shifts superior to 1000 km (Supplementary Fig. 16b). These important longitudinal shifts corroborate existing projections[22,38,39] and differ from trivial poleward shifts due to temperature increase, reflecting more complex spatial rearrangements of the other environmental drivers (Supplementary Fig. 12). The average displacement speed of the provinces' centroids is 76 ± 79 $km.dec^{-1}$ (latitudinally mean of 34 ± 82 $km.dec^{-1}$, longitudinally 59 ± 82 $km.dec^{-1}$).

Projected shifts in phytoplankton enriched provinces corroborate previously published shifts of North Pacific phytoplankton biomes: provinces C4 and C9 are projected to shift respectively at speeds of 118 $km.dec^{-1}$ and 195 $km.dec^{-1}$ comparable to 100 $km.dec^{-1}$ and 200 $km.dec^{-1}$ for the subtropical and tropical biomes of Polovina et al.[39].

For all size fractions, climate change would lead to a poleward expansion of tropical and equatorial provinces at the expense of temperate provinces (Supplementary information 4, Supplementary Table 2, Supplementary Figs. 14 and 17). This is illustrated by the temperate province F5 of size fraction 180-2000 (Supplementary Fig. 16), which is projected to shrink in the five major basins. In the North Atlantic, its centroid would move approximately 800 km to the northeast (Supplementary Fig. 16c). Similar trends are found comparing present day and end of the century consensus maps (Supplementary information 2, Supplementary Fig. 17).

We calculate a dissimilarity index (equation (3)) at each grid point between probabilities of future and present *dominant* provinces for all size fractions combined (Fig. 4a). Large dissimilarities are obtained over northern (25° to 60°) and symmetrically southern (-25 to -60°) temperate regions (mean of 0.29 and 0.24 respectively) mostly reflecting

the poleward retraction of temperate provinces (red arrows, Fig. 4a). In austral and equatorial regions, despite important environmental changes (Supplementary Fig. 12) and previously projected changes in diversity[28–30] and biomass[40], the contemporary provinces remain the most probable at the end of the century (mean dissimilarities of 0.18 and 0.02 respectively).

To further study the future decoupling between provinces of different size fractions, we analyze the assemblages of *dominant* provinces of each size fraction. By using two differently stringent criteria, from 45.3 to 57.1% of ocean surface, mainly located in temperate regions, would be inhabited in 2090-99 by assemblages that exist elsewhere in 2006-15 (Fig. 4b versus Fig. 4c). Contemporary assemblages would disappear on 3.5 to 3.8% of the surface, and, conversely, novel assemblages, not encountered today, would cover 2.9 to 3.0% of the surface. While these changes are limited to a relatively modest area, they include important economic zones (Fig. 4b, Supplementary Fig. 19). Over 41.8% to 51.8% of the surface of the main fisheries and 41.2% to 54.2% of Exclusive Economic Zones, future assemblages would differ from those present today (Supplementary Fig. 19).

**Future changes in the distribution of grazers and nitrogen-fixing bacteria**

In order to elucidate the potential biogeochemical impact of biogeographical restructuring, we focus on compositional changes among copepods and nitrogen-fixing bacteria (a.k.a, diazotrophs), two groups considered important for the carbon and nitrogen cycles[41,42] that are well represented among the Tara Oceans environmental genomes. Focusing on marine areas where *dominant* provinces are projected to be replaced, we compare the present and future distribution of environmental genomes corresponding to 198 copepods and 27 diazotrophs[32,33].

Copepods are cosmopolitan small crustaceans. These abundant grazers contribute to the biological pump and their body size is considered to be a key trait for carbon export[41]. They feed on smaller plankton[41] and are prey to higher trophic levels. We characterize the composition of provinces using 198 environmental genomes detected in at least 5 samples and annotated as Marine Hexanauplia of clade A and B. They are further divided into five subgroups based on their differential abundances across the large size classes (>5 μm): 8 mesozooplankton clade A, 19 unclassified clade A, 71

186 microzooplankton clade A, 10 unclassified clade B and 90 microzooplankton clade B.
187 Therefore, large copepods are preferentially from clade A in our data.
188 The relative abundances of unclassified clade B in size class 20-180 μm (Fig. 3e) and of
189 mesozooplankton clade A in size class 180-2000 μm, (Supplementary Fig. 20a) are
190 projected to increase in regions where the temperate province is replaced by the
191 tropico-equatorial province. In areas where the polar province is replaced by the
192 temperate province, a greater relative abundance in microzooplankton clade A (1% to
193 10%) (Fig. 3e) is projected. No significant compositional differences in the provinces of
194 size fraction 5-20 μm are found (Supplementary Fig. 20b). These results highlight
195 potential significant compositional shifts by the end of the century in the different clades
196 and sizes of main grazers.
197 Diazotrophy, the biotic fixation of atmospheric nitrogen, is an important process for both
198 nitrogen and carbon cycles. It supports biological productivity in the nitrogen-limited
199 tropical oceans[42]. Marine diazotrophs include cyanobacteria (*e.g. Trichodesmium*)
200 described as the principal nitrogen fixers[43] and various heterotrophic bacterial
201 diazotrophs (HBDs) that lack cultured representatives or *in situ* imaging[33,44]. Forty-eight
202 of the bacterial environmental genomes are diazotrophs (8 cyanobacteria and 40
203 heterotrophic bacterial diazotrophs (HBDs)), encapsulating 92% of the metagenomic
204 signal for known *nifH* genes (a reference marker for nitrogen fixation[45]) at the surface of
205 the oceans. Twenty-seven are found in at least 5 samples and have been used for the
206 analysis.
207 In size fraction 0.8-5 μm, we project significantly higher relative abundances in
208 cyanobacteria in the tropico-equatorial regions of the Pacific ocean (C9 to C11 and C4,
209 Fig. 3f), which might point towards an increase in nitrogen fixation in this region as
210 previously suggested by other models[42]. Supporting this result, we find similar
211 significant compositional changes towards an increase in cyanobacteria in size fraction
212 5-20 μm (Supplementary Fig. 21c). We also project significant compositional changes
213 for some clades of HBDs (*e.g.* increase in gammaproteobacteria: C8 to C3, Fig. 3f)
214 though no global trend can be identified here. In the other size classes (20-180, 180-
215 2000 and 0.22-3 μm) compositional changes are not significant (Supplementary Fig.
216 22). To summarize, although we cannot estimate nitrogen fixation rates using genomic

data alone, genomic measurements of nitrogen-fixing cyanobacteria are in agreement with an increase in nitrogen fixation in the tropics, echoing results from other models[42].

**Drivers of plankton biogeography reorganization**

We quantify the relative importance of environmental predictors (sea surface temperature, salinity, dissolved silica, phosphate, nitrate, iron and seasonality of nitrate) into niche definition and in driving future changes of the structure of plankton biogeography (equation (4)). Among these environmental properties, temperature is the first influential parameter (for 19 niches out of 27) but only at 22.6% on average (Supplementary Fig. 22a).

The relative impact of each environmental parameter is calculated[22] for each site presenting a significant dissimilarity between 2006-15 and 2090-99 (Fig. 5a). Overall, SST would be responsible for the reorganization of the provinces at 50% followed by Phosphate (11%) and Salinity (10.3%) (Supplementary Fig. 23). Over the majority of the ocean, SST is the primary driver of the reorganization (Fig. 5a). In some regions, salinity (e.g. eastern North Atlantic) and Phosphate (e.g. equatorial region) dominate (Fig. 5a). When excluding the effect of SST, salinity and phosphate become the primary drivers of the reorganization of the provinces (Fig. 5b). The impact of SST varies across size classes with a significantly higher contribution in large size classes (>20 µm) compared to the small ones (mean of ~73% versus ~49%, t-test $p<0.05$; Fig. 5c). Though the contribution of combined nutrients to niche definition is similar for small and large size classes (mean of ~56% versus ~61%, Supplementary Fig. 22, Supplementary Table 3), their future projected variations have a higher relative impact on the reorganization of biogeographies of small organisms (mean of ~39% versus ~20%, t-test $p<0.05$, Supplementary Fig. 22, Supplementary Table 3). For instance, in the tropical zone, the shrinkage of the equatorial province C9 (size fraction 0.8-5 µm, Fig. 2b,d, Supplementary Fig. 24e) is driven at 24% by reduction of dissolved phosphate concentrations and at 25% by SST increase. In contrast, SST drives at 56% the shrinkage of the temperate province F5 (size fraction 180-2000 µm, Supplementary Fig. 24d). Finally, non-poleward shifts are found only within small size fractions (<20 µm) (Supplementary Figs. 14, 15) highlighting differential responses to nutrients and SST

247 changes between large and small organisms, the latter being enriched in phytoplankton
248 that directly rely on nutrient supplies.

249 **Discussion**

250 We propose a novel partitioning of the ocean in plankton size dependent *climato-*
251 *genomic* provinces, complementing previous efforts based on other bio-physico-
252 chemical data[9–11]. Though initially built at genomic scale, our biogeographies
253 paradoxically reveal basin scale provinces that are larger than BGCP[10] and Fay and
254 McKingley biomes[9]. These provinces are probably relatively stable across seasons
255 suggesting limited effects of seasonality on the position of frontiers of BGCPs
256 provinces[10]. We propose that this apparent paradox emerges from the combination of
257 the scale, nature and resolution of sampling. First, two proximal samples from the *Tara*
258 Oceans expedition are separated by ~300 km on average sampled over three years.
259 This relatively large spatio-temporal scale overlies shorter scale compositional
260 variations previously observed[5,6]. Second, our estimates of plankton community
261 dissimilarities are highly resolutive as they are computed at genomic scale with billions
262 of small DNA fragments[11,18] thus smoothing out the more discrete species level signal.
263 Together, from these combinations of processes and patterns occurring at multiple
264 scales emerge basin scale provinces associated with coherent environmental niches
265 and signature genomes.

266 These *climato-genomic* provinces are structured in broad latitudinal bands with smaller
267 organisms (<20 µm) displaying more complex patterns and partially decoupled from
268 larger organisms. This decoupling is the result of distinct statistical links between
269 provinces based on organism size fractions and environmental parameters and could
270 reflect their respective trophic modes[35].

271 Complex changes of the parameters defining the niches are projected under climate
272 change leading to the reorganization of size-dependent provinces. Assuming a constant
273 relationship to environmental drivers that define the *climato-genomic* provinces, climate
274 change is projected to restructure them over approximately 50% of surface oceans
275 south of 60°N by the end of the century (Fig. 4). The largest reorganization is detected
276 in subtropical and temperate regions in agreement with other studies[29,39] and is
277 accompanied by appearance and disappearance of size-fractionated provinces'

assemblages. Out of contemporary range and novel environmental conditions are projected for tropico-equatorial and austral regions. While some studies extrapolate important diversity and biomass changes in these zones[28–30,40], here we project shifts of their boundaries and maintenance of their climatic label. The present approach does not account for putative changes in community composition or the emergence of novel niches over these regions for which novel environmental selection pressure is expected. Despite these limitations, genomic data allow us to project compositional shifts due to the reorganization of the provinces at a high phylogenetic and functional resolution. Large (size class 180-2000 µm) and small (size class 20-180 µm) copepods are expected to be in greater relative abundance in subtropical and subpolar regions, respectively. Though the *Tara* Oceans environmental genomes collection might not reflect the full diversity in copepods, this projected restructuration of the communities in small and large copepods could modify carbon export as grazers' size is a key trait for this process[41]. Secondly, it might lead to novel prey-predator interactions *e.g.* in regions where new assemblages of communities are projected.

Important compositional shifts among most abundant marine nitrogen-fixing bacteria are also found. The relative share of nitrogen-fixing cyanobacteria is projected to increase in tropico-equatorial regions congruent with modeling studies[42]. Though their contribution to nitrogen fixation is not characterized, heterotrophic bacterial diazotrophs are abundant in genomic samples[33] and significant compositional shifts in certain clades are reported here. Ultimately, further studies associating omics and physico-chemical data should be informative for biogeochemical modeling of nitrate fixation rates and carbon export fluxes.

Overall, our projections for the end of the century do not take into account possible future changes of major bio-physico-chemical factors such as the dynamics of community mixing, trophic interactions through transport[46], the dynamics of the genomes[13–15] (adaptation or acclimation) and biomass variations[40]. New sampling in current and future expeditions[47], as well as ongoing technological improvements in bio-physico-chemical characterization of seawater samples[32,47,48], will soon refine functional[16,49], environmental (micronutrients[50]) and phylogenetic[32] characterization of plankton ecosystems for various biological entities (genotypes, species or communities)

and spatio-temporal scales[47]. Ultimately, integrating this varied information will allow a better understanding of the conditions of emergence of ecological niches in the seascape and their response to a changing ocean.

## References

1. Field, C. B., Behrenfeld, M. J., Randerson, J. T. & Falkowski, P. Primary production of the biosphere: Integrating terrestrial and oceanic components. *Science (80-. ).* (1998). doi:10.1126/science.281.5374.237
2. Guidi, L. *et al.* Plankton networks driving carbon export in the oligotrophic ocean. *Nature* (2016). doi:10.1038/nature16942
3. Henson, S. A. *et al.* Detection of anthropogenic climate change in satellite records of ocean chlorophyll and productivity. *Biogeosciences* (2010). doi:10.5194/bg-7-621-2010
4. Azam, F. *et al.* The Ecological Role of Water-Column Microbes in the Sea. *Mar. Ecol. Prog. Ser.* (1983). doi:10.3354/meps010257
5. Saab, M. A. abi. Day-to-day variation in phytoplankton assemblages during spring blooming in a fixed station along the Lebanese coastline. *J. Plankton Res.* (1992). doi:10.1093/plankt/14.8.1099
6. Djurhuus, A. *et al.* Environmental DNA reveals seasonal shifts and potential interactions in a marine community. *Nat. Commun.* (2020). doi:10.1038/s41467-019-14105-1
7. Kavanaugh, M. T. *et al.* Seascapes as a new vernacular for pelagic ocean monitoring, management and conservation. *ICES J. Mar. Sci.* (2016). doi:10.1093/icesjms/fsw086
8. Longhurst, A. R. *Ecological Geography of the Sea*. *Ecological Geography of the Sea* (2007). doi:10.1016/B978-0-12-455521-1.X5000-1
9. Fay, A. R. & McKinley, G. A. Global open-ocean biomes: Mean and temporal variability. *Earth Syst. Sci. Data* (2014). doi:10.5194/essd-6-273-2014
10. Reygondeau, G. *et al.* Dynamic biogeochemical provinces in the global ocean. *Global Biogeochem. Cycles* (2013). doi:10.1002/gbc.20089
11. Richter, D. J. *et al.* Genomic evidence for global ocean plankton biogeography shaped by large-scale current systems. *bioRxiv* 867739 (2020).

doi:10.1101/867739

12. Dutkiewicz, S. *et al.* Dimensions of marine phytoplankton diversity. *Biogeosciences* (2020). doi:10.5194/bg-17-609-2020
13. Hellweger, F. L., Van Sebille, E. & Fredrick, N. D. Biogeographic patterns in ocean microbes emerge in a neutral agent-based model. *Science (80-. ).* (2014). doi:10.1126/science.1254421
14. Laso-Jadart, R. *et al.* Investigating population-scale allelic differential expression in wild populations of Oithona similis (Cyclopoida, Claus, 1866). *Ecol. Evol.* (2020). doi:10.1002/ece3.6588
15. Delmont, T. O. *et al.* Single-amino acid variants reveal evolutionary processes that shape the biogeography of a global SAR11 subclade. *Elife* (2019). doi:10.7554/eLife.46497
16. Carradec, Q. *et al.* A global ocean atlas of eukaryotic genes. *Nat. Commun.* (2018). doi:10.1038/s41467-017-02342-1
17. Salazar, G. *et al.* Gene Expression Changes and Community Turnover Differentially Shape the Global Ocean Metatranscriptome. *Cell* (2019). doi:10.1016/j.cell.2019.10.014
18. Alberti, A. *et al.* Viral to metazoan marine plankton nucleotide sequences from the Tara Oceans expedition. *Sci. Data* (2017). doi:10.1038/sdata.2017.93
19. Pesant, S. *et al.* Open science resources for the discovery and analysis of Tara Oceans data. *Sci. Data* (2015). doi:10.1038/sdata.2015.23
20. Karsenti, E. *et al.* A holistic approach to marine Eco-systems biology. *PLoS Biol.* (2011). doi:10.1371/journal.pbio.1001177
21. Duarte, C. M. Seafaring in the 21st century: The Malaspina 2010 circumnavigation expedition. *Limnology and Oceanography Bulletin* (2015). doi:10.1002/lob.10008
22. Barton, A. D., Irwin, A. J., Finkel, Z. V. & Stock, C. A. Anthropogenic climate change drives shift and shuffle in North Atlantic phytoplankton communities. *Proc. Natl. Acad. Sci.* (2016). doi:10.1073/pnas.1519080113
23. Benedetti, F., Guilhaumon, F., Adloff, F. & Ayata, S. D. Investigating uncertainties in zooplankton composition shifts under climate change scenarios in the

Mediterranean Sea. *Ecography (Cop.).* (2018). doi:10.1111/ecog.02434

24. Beaugrand, G. *et al.* Prediction of unprecedented biological shifts in the global ocean. *Nat. Clim. Chang.* **9**, 237–243 (2019).
25. McMahon, K. W., McCarthy, M. D., Sherwood, O. A., Larsen, T. & Guilderson, T. P. Millennial-scale plankton regime shifts in the subtropical North Pacific Ocean. *Science (80-. ).* (2015). doi:10.1126/science.aaa9942
26. Pinsky, M. L., Worm, B., Fogarty, M. J., Sarmiento, J. L. & Levin, S. A. Marine taxa track local climate velocities. *Science (80-. ).* (2013). doi:10.1126/science.1239352
27. Bopp, L. *et al.* Multiple stressors of ocean ecosystems in the 21st century: Projections with CMIP5 models. *Biogeosciences* (2013). doi:10.5194/bg-10-6225-2013
28. Thomas, M. K., Kremer, C. T., Klausmeier, C. A. & Litchman, E. A global pattern of thermal adaptation in marine phytoplankton. *Science (80-. ).* (2012). doi:10.1126/science.1224836
29. Busseni, G. *et al.* Large scale patterns of marine diatom richness: Drivers and trends in a changing ocean. *Glob. Ecol. Biogeogr.* (2020). doi:10.1111/geb.13161
30. Ibarbalz, F. M. *et al.* Global Trends in Marine Plankton Diversity across Kingdoms of Life. *Cell* (2019). doi:10.1016/j.cell.2019.10.008
31. Hutchinson, G. E. Concludig remarks. *Cold Spring Harb. Symp. Quant. Biol.* (1957).
32. Delmont, T. O. *et al.* Functional repertoire convergence of distantly related eukaryotic plankton lineages revealed by genome-resolved metagenomics. *bioRxiv* 2020.10.15.341214 (2020). doi:10.1101/2020.10.15.341214
33. Delmont, T. O. *et al.* Heterotrophic bacterial diazotrophs are more abundant than their cyanobacterial counterparts in metagenomes covering most of the sunlit ocean. *bioRxiv* 2021.03.24.436778 (2021). doi:10.1101/2021.03.24.436778
34. Boyer, T. P. *et al.* WORLD OCEAN DATABASE 2013, NOAA Atlas NESDIS 72. *Sydney Levitus, Ed.; Alexey Mishonoc, Tech. Ed.* (2013). doi:10.7289/V5NZ85MT
35. Sunagawa, S. *et al.* Tara Oceans: towards global ocean ecosystems biology. *Nature Reviews Microbiology* (2020). doi:10.1038/s41579-020-0364-5

36. Moon, K. R. *et al.* Visualizing structure and transitions in high-dimensional biological data. *Nat. Biotechnol.* (2019). doi:10.1038/s41587-019-0336-3

37. van Vuuren, D. P. *et al.* The representative concentration pathways: An overview. *Clim. Change* (2011). doi:10.1007/s10584-011-0148-z

38. Marinov, I. *et al.* North-South asymmetry in the modeled phytoplankton community response to climate change over the 21st century. *Global Biogeochem. Cycles* (2013). doi:10.1002/2013GB004599

39. Polovina, J. J., Dunne, J. P., Woodworth, P. A. & Howell, E. A. Projected expansion of the subtropical biome and contraction of the temperate and equatorial upwelling biomes in the North Pacific under global warming. *ICES J. Mar. Sci.* (2011). doi:10.1093/icesjms/fsq198

40. Flombaum, P., Wang, W. L., Primeau, F. W. & Martiny, A. C. Global picophytoplankton niche partitioning predicts overall positive response to ocean warming. *Nat. Geosci.* (2020). doi:10.1038/s41561-019-0524-2

41. Richardson, A. J. In hot water: zooplankton and climate change. *ICES J. Mar. Sci.* **65**, 279–295 (2008).

42. Wrightson, L. & Tagliabue, A. Quantifying the Impact of Climate Change on Marine Diazotrophy: Insights From Earth System Models . *Frontiers in Marine Science* **7**, 635 (2020).

43. Luo, Y.-W. *et al.* Database of diazotrophs in global ocean: abundance, biomass and nitrogen fixation rates. *Earth Syst. Sci. Data* **4**, 47–73 (2012).

44. Zehr, J. P. & Capone, D. G. Changing perspectives in marine nitrogen fixation. *Science (80-. ).* **368**, eaay9514 (2020).

45. Gaby, J. C. & Buckley, D. H. A comprehensive evaluation of PCR primers to amplify the nifH gene of nitrogenase. *PLoS One* **7**, (2012).

46. Iudicone, D. Some may like it hot. *Nature Geoscience* (2020). doi:10.1038/s41561-020-0535-z

47. Gorsky, G. *et al.* Expanding Tara Oceans Protocols for Underway, Ecosystemic Sampling of the Ocean-Atmosphere Interface During Tara Pacific Expedition (2016–2018). *Front. Mar. Sci.* (2019). doi:10.3389/fmars.2019.00750

48. Istace, B. *et al.* de novo assembly and population genomic survey of natural yeast

isolates with the Oxford Nanopore MinION sequencer. *Gigascience* (2017). doi:10.1093/gigascience/giw018

49. Busseni, G. *et al.* Meta-Omics Reveals Genetic Flexibility of Diatom Nitrogen Transporters in Response to Environmental Changes. *Mol. Biol. Evol.* (2019). doi:10.1093/molbev/msz157

50. Grand, M. M. *et al.* Developing autonomous observing systems for micronutrient trace metals. *Frontiers in Marine Science* (2019). doi:10.3389/fmars.2019.00035

## Acknowledgments

PF was supported by a CFR doctoral fellowship and the *NEOGEN impulsion* grant from the Direction de la recherche fondamentale (DRF) of the CEA. This study received funding from the European Union's Horizon 2020 Blue Growth research and innovation program under grant agreement No 862923 (project AtlantECO). We thank the LSCE (Laboratoire des Sciences du Climat et de l'Environnement, CEA) for providing Earth System Models outputs, Tilla Roy for preparation of the data, LAGE (Laboratoire d'Analyses Génomiques des Eucaryotes, CEA) members for stimulating discussions on this project, Mahendra Mariadassou, Sakina Dorothée Ayata and Bruno Hay Mele for discussions on statistics and climate envelope models, Laurent Bopp for initial discussions on this project and on climate models and Noan Le Bescot (TernogDesign) for help with the Figures. We thank all members of the *Tara* Oceans consortium for maintaining a creative environment and for their constructive criticism. *Tara* Oceans would not exist without the *Tara* Ocean Foundation and the continuous support of 23 institutes (https://oceans.taraexpeditions.org/).

This article is contribution number XX of *Tara* Oceans.

## Competing interests

The authors declare no competing interests.

## Author contributions

PF, OJ and MG conceived the study. MV wrote the bias correction algorithm. PF computed the results, compiled and analyzed the data. PF wrote the initial draft of the paper. JL, OJ and MG conducted a preliminary study. PF, OJ, MG, MV, TD, DI, and PW discussed the results and contributed to write the paper.

# Online content

All data and codes used are available at http://www.genoscope.cns.fr/tara/SourceCodes/NCLIM-20102618_codes.tar.gz

# Materials and methods

## Genomic provinces of plankton

Environmental niches are computed for trans-kingdom plankton genomic provinces from Richter et al.[11]. They consist of the clustering of metagenomic dissimilarity matrices (based on the amount of DNA k-mers shared between pairs of samples) from 6 available size fractions with sufficient metagenomic data from the *Tara* Oceans dataset. The six size fractions (0-0.2, 0.22-3, 0.8-5, 5-20, 20-180 and 180-2000 µm) represent major plankton groups. Two large size classes (180-2000 µm and 20-180 µm) are enriched in zooplankton dominated by arthropods (mainly copepods) and cnidarians. They are expected to directly depend on smaller eukaryotes as they feed on them. Size classes 5-20 µm and 0.8-5 µm are enriched in smaller eukaryotic algae, such as dynophytes (5-20 µm), pelagophytes and haptophytes (0.8-5 µm). The distribution of these photoautotrophs presumably depends on nutrient availability. Finally, size classes 0.22-3 µm and 0-0.2 µm are respectively enriched in bacteria and viruses. Bacteria are characterized by a wide range of trophisms including autotrophy (cyanobacteria), mixotrophy and heterotrophy, while viruses are mainly parasites. Within each size fraction (from large to small), there are respectively 8, 8, 11, 6, 6 and 8 (48 in total) provinces defined in Richter et al.[11] formed by *Tara* Oceans metagenomes (644 metagenomes sampled either at the surface (SUR) or at the Deep Chlorophyll Maximum (DCM) across 102 sites). The clustering of individual size fractions is independent.

## Genome signature of the provinces

We analyzed the distribution of 713 eukaryotic and 1888 prokaryotic genomes[32,33] within the genomic provinces. These genomes are Metagenome-Assembled Genomes (MAGs) obtained from *Tara* Oceans metagenomes. For each size class, we select MAGs that are present (according to a criteria defined in Delmont et al.[32]) in at least 5 samples. We computed an index of presence enrichment of MAGs within provinces as the Jaccard index[51], defined as follows:

$$J = \frac{M_{11}}{M_{11}+M_{01}+M_{10}} \qquad (1)$$

$M_{11}$ is the number of samples where the MAG is present and match a sample of the province. $M_{01}$ and $M_{10}$ are respectively the number of samples where the MAG is not present in a sample of the province and inversely. A MAG is considered to be signature of a province if the Jaccard index is superior to 0.5 with this province and inferior to 0.1 for all other provinces of the given size class (Fig. 1 and Supplementary Fig. 3).

## World Ocean Atlas data

Physicochemical parameters proposed to have an impact on plankton genomic provinces[11] are used to define environmental niches: sea surface temperature (SST), salinity (Sal); dissolved silica (Si), nitrate ($NO_3$), phosphate ($PO_4$), iron (Fe), and a seasonality index of nitrate (SI $NO_3$). With the exception of Fe and SI $NO_3$, these parameters are extracted from the gridded World Ocean Atlas 2013 (WOA13)[34]. Climatological Fe fields are provided by the biogeochemical model PISCES-v2[52]. The seasonality index of nitrate is defined as the range of nitrate concentration in one grid cell divided by the maximum range encountered in WOA13 at the *Tara* Oceans sampling stations. All parameters are co-located with the corresponding stations and extracted at the month corresponding to the *Tara* Oceans sampling. To compensate for missing physicochemical samples in the *Tara* Oceans *in situ* data set, climatological data (WOA) are preferred. The correlation between in situ samples and corresponding values extracted from WOA are high ($r^2$: SST: 0.96, Sal: 0.83, Si: 0.97, $NO_3$: 0.83, $PO_4$: 0.89). In the absence of corresponding WOA data, a search is done within 2° around the sampling location and values found within this square are averaged.

Nutrients, such as $NO_3$ and $PO_4$, display a strong collinearity when averaged over the global ocean (correlation of 0.95 in WOA13) which could complicate disentangling their respective contributions to niche definition. However, observations and experimental data allow identification of limiting nutrients at regional scale characterized by specific plankton communities[53]. The projection of niches into future climate would yield spurious results when the present-day collinearity is not maintained[54] but there is up to now no evidence for large scale changes in global nutrient stoichiometry[55].

## Earth System Models and bias correction

Outputs from 6 Earth System Models (ESM) (Supplementary Table 2) are used to project environmental niches under greenhouse gas concentration trajectory RCP8.5[37]. Environmental drivers are extracted south of 60° north for present day (2006-2015) and end of century (2090-2099) conditions for each model and the multi-model mean is computed. A bias correction method, the Cumulative Distribution Function transform, CDFt[56], is applied to adjust the distributions of SST, Sal, Si, $NO_3$ and $PO_4$ of the multi-model mean to the WOA database. CDFt is based on a quantile mapping (QM) approach to reduce the bias between modeled and observed data, while accounting for climate change. Therefore, CDFt does not rely on the stationarity hypothesis and present and future distributions can be different. CDFt is applied on the global fields of the mean model simulations. By construction, CDFt preserves the ranks of the simulations to be corrected. Thus, the spatial structures of the model fields are preserved.

## Environmental niche models: training, validation and projections

Provinces with similar metagenomic content are retrieved from Richter et al.[11]. From a total of 48 initial provinces, 10 provinces are removed either because they are represented by too few samples (7 out of 10) or they are found in environments not resolved by ESMs (*e.g.* lagoons of Pacific Ocean islands, 3 out of 10). This narrows down the number of samples from 644 to 595 metagenomes. Four machine learning methods are applied to compute environmental niches for each of the 38 provinces: Gradient Boosting Machine (gbm)[57], Random Forest (rf)[58], fully connected Neural Networks (nn)[59] and Generalized Additive Models (gam)[60]. Hyper parameters of each technique (except gam) are optimized. These are (1) for gbm, the interaction depth (1, 3 and 5), learning rate (0.01, 0.001) and the minimum number of observations in a tree node (1 to 10); (2) for rf, the number of trees (100 to 900 with step 200 and 1000 to 9000 with step 2000) and the number of parameters used for each tree (1 to 7); (3) for nn, the number of layers of the network (1 to 10) and the decay ($1.10^{-4}$ to $9.10^{-4}$ and $1.10^{-5}$ to $9.10^{-5}$). For gam the number of splines is set to 3, respectively 2 only when not enough points are available (for fraction 0-0.2, 65 points). R packages gbm (2.1.3),

randomForest (4.6.14), mgcv (1.8.16) and nnet (7.3.12) are used for gbm, rf, nn and gam models.

To define the best combination of hyper parameters for each model, we perform random cross-validation by training the model on 85% of the dataset randomly sampled and by calculating the Area Under the Curve[61] (AUC) on the 15% remaining points of the dataset. This process is repeated over 30 random subsets of the entire training set for each combination of hyperparameters. We work in a presence/absence framework *i.e.* for each province separately the dataset consists of the variable to predict ("presence" or not of the province in the sample) and the predictors consisting of the environmental variables for each sample. A fixed probability threshold of 0.5 for presence/absence detection is used to calculate the AUC, *i.e.* samples with P, the probability of presence calculated by the model, superior to 0.5 are assigned to 1 and inversely samples with P inferior to 0.5 are assigned to 0. Fixing the probability threshold allows optimization of all models according to this threshold so that within a size fraction the *dominant* province has a reasonably high probability of presence (at least in regions with similar environmental parameters to the training dataset) and for the four types of models we use (gbm, nn, rf and gam). The best combination of hyper parameters is the one for which the mean AUC over the cross-validation is the highest. A model is considered valid if at least 3 out of the 4 techniques have a mean AUC superior to 0.65, which is the case for 27 out of the 38 provinces (Supplementary Fig. 2a). A climatic annotation is given to the 27 validated niches (Supplementary Table 2). Final models are trained on the full dataset and only the techniques that have a mean AUC higher than 0.65 are considered to make the projections. The vast majority (23) of the 27 validated niches is validated by all four models and 4 by only 3 models. Relative influences of each parameter in defining environmental niches are calculated using the feature_importance function from the DALEX R package[62] for all four statistical methods (Supplementary Fig. 22a). To evaluate the consistency and coherence of environmental niche models, we first make global projections on the 2006-13 WOA2013 climatology. Projections are consistent with sampling regions for provinces encompassing vast oceanic areas. For example, the genomic province sampled in temperate Atlantic regions of size fraction 180-2000 µm is projected to be present in the north and south

584 temperate Atlantic but also other temperate regions (Supplementary Fig. 4). For model
585 training and projections, physicochemical variables are scaled to have a mean of 0 and
586 a variance of 1. For this scaling, the mean and standard deviation of each WOA13
587 variable (+ PISCES-v2 Fe) co-localized with *Tara* Oceans stations with a value available
588 are used. This standardization procedure allows for better performance of nn models.
589 Finally, as statistical models often disagree on projection sets whereas they give similar
590 predictions on the training set (Supplementary Fig. 6, 7), we use the ensemble model
591 approach for global-scale projections of provinces[63] *i.e.* the mean projections of the
592 validated machine learning techniques.

593 **Combined size class provinces and ocean partitioning comparisons**

594 To combine all size classes' provinces, we use the PHATE algorithm[36,64] from the R
595 package phateR. This algorithm allows visualization of high dimensional data in the
596 requested number of dimensions while best preserving the global data structure[64]. We
597 choose to train PHATE separately on WOA13 projections and present day and end of
598 century projections including presence probabilities of *non dominant* provinces. We use
599 3 dimensions and set hyper parameter k-nearest neighbors (knn) and decay
600 respectively to 1000 for WOA13 and 2000 for model data as in this case there are twice
601 as many points. The hyper parameter knn reflects the degree to which the mapping of
602 PHATE from high to low dimensionality should respect the global features of the data.
603 We argue that 1000 and 2000 are good choices as it will be sufficient to have a highly
604 connected graph, conserve global structure, allow visualization of structures of the size
605 of the provinces (mean number of points in a province: 4867) and have a reasonable
606 computational time. Decay is set to 20 in both cases. Then we cluster the resulting
607 distance matrix using the k-medoïds algorithm[65] and the silhouette average width
608 criteria[66] is used as an indicator of good fit. The silhouette criterion is maximal for 2, 3
609 and 4 clusters and 2 peaks are found at 7 and 14 clusters (the peak at 7 is slightly less
610 high than the one at 14, data not shown). We choose to present the 4 and 7 cluster
611 geographical patterns as they seem more relevant with respect to the resolutions of our
612 environmental datasets (WOA13 and climate models). We compare the three polar
613 clusters of the 7 cluster geographical patterns with Antarctic Circumpolar Currents
614 fronts[67] by overlying them on the map (black lines Supplementary Fig. 5b).

To visualize the global biogeography structure, the resulting 3 vectors of PHATE are plotted using an RGB color code. Each coordinate of each vector is respectively assigned to a given degree of color component between 0 and 255 (8 bits red, green or blue) using the following formula (Supplementary Figs. 5, 17):

$$C\_col(i) = \frac{C(i) - \min\left(C(1), C(2), C(3)\right)}{\max\left(C(1), C(2), C(3)\right) - \min\left(C(1), C(2), C(3)\right)} * 255 \quad (2)$$

$C(i)$ is the ith component of the PHATE axes. Respectively, components 1, 2 and 3 are assigned to red, green and blue.

To compare the six size fraction provinces, the combined size class with existing biogeochemical partitions of the oceans[9,10] and with each other, we use the adjusted rand index[68] (Supplementary Fig. 8-10) and overlay their masks above our partitions. In this case, presence probabilities of *dominant* provinces are not used anymore. Instead, each ocean grid point is assigned to the *dominant* provinces or the phate clusters.

**Centroids and migration shifts**

The centroid of each province is defined as the average latitude and longitude for which the probability of presence is superior to 0.5 and weighted by both the probability of presence at each grid point and the grid cell area. It is calculated for both present day conditions and end of the century conditions. The migration shift is calculated as the distance between the present day and the end of the century centroids considering the earth as a perfect sphere of radius 6371 km. For consistency (*i.e.* avoid long distance aberrant shifts), it is only calculated for provinces with an area of dominance larger than $10^6$ km$^2$ in the given basin.

**Bray-Curtis dissimilarity index**

Climate change impact on global projections is calculated at each grid point as the Bray-Curtis dissimilarity index[69,70] defined as follows:

$$BC = \frac{\sum_n \left| P_n^{future} - P_n^{present} \right|}{\sum_n \left| P_n^{future} + P_n^{present} \right|} \quad (3)$$

Where ($P_n^{present}$ and $P_n^{future}$) are respectively the probability of presence of the province n in present day and at the end of the century. Only the probabilities of *dominant* provinces are non-null and all others are set to zero. The mask of main fisheries[71]

(chosen as the first 4 deciles) and Exclusive Economical Zones[72] is overlaid on the Bray-Curtis map.

**Change in province assemblages**

A province assemblage is defined as the assemblage of *dominant* provinces of each size fraction at a given grid point of the considered ocean. We consider two criteria of change in province assemblage between present day and end of the century conditions. The first one, more straightforward and less stringent, considers that a province assemblage occurs when a change of *dominant* province is found in at least one size fraction. In a more stringent way, a change of assemblage is considered significant for $BC > \frac{1}{6}$ (previous section). This threshold corresponds to an idealized case where each *dominant* province has a probability of one and a change of *dominant* province is found in only one size fraction. For example, the *dominant* province assemblage goes from vector (F5,E6,D3,C8,B7,A7) (with the size fractions in decreasing order) corresponding to all temperate provinces to vector (F8,E6,D3,C8,B7,A7). This example corresponds to the replacement of the temperate province of size fraction 180-2000 µm (F5) by the tropico-equatorial province (F8). This criterion allows us to discard assemblage changes for which the changes in probability of presence of *dominant* provinces are very low. With this criterion, only a small oceanic area is found to have no changes of assemblage (Fig. 4c light blue zones).

**Composition of provinces in bacterial diazotrophs and marine copepods**

We characterize the composition in Marine Hexanauplia (copepods) and marine diazotrophs of provinces by considering the mean relative abundances of groups of MAGs[32,33] characterized taxonomically (for both copepods and diazotrophs) and by size (for copepods) in each province for all size fractions except the viral one (for diazotrophs) and for size fractions >5 µm (for Marine Hexanauplia). Marine Hexanauplia are annotated taxonomically (either as belonging to clade A (109 MAGs) or clade B (105 MAGs)) from which 198 are found in at least 5 samples that we use (98 clade A and 100 clade B). To attribute a preferential size class to these MAGs, mean relative abundances over all sites of each of them are compared across size fraction 180-2000, 20-180 and 5-20 µm using Welch ANOVA[73] (p-value<0.05). When the Welch ANOVA

test is significant the MAG is either annotated as mesozooplankton (when most abundant in size class 180-2000 µm) or microzooplankton (when most abundant in size class 20-180 or 5-20 µm). When the Welch ANOVA test is not significant, the MAG is annotated as unclassified. Then for each group of MAG (defined by the preferential size class plus the clade), the mean of the sum over the MAGs from this group is calculated in each province to characterize the province. The same procedure is applied for 27 out of 48 bacterial diazotrophs (present in at least 5 samples) from the prokaryotic MAG collection[33] distinguishing groups at the phylum level (Gammaproteobacteria n=8, Cyanobacteria n=8, Deltaproteobacteria n=2, Alphaproteobacteria n=4, Planctomycetes n=3, Verrucomicrobiota n=2). Finally, significant differential composition between provinces are annotated using Holm corrected[74] pairwise Mann-Whitney U test[75] ($p<0.05$ for significance) comparing the abundance distributions of each group of either diazotrophs or copepods between each pair of provinces from a same size class.

**Driver analysis**

To assess the relative importance of each driver in province changes, the methodology from Barton et al.[24] is adopted. For a set N of n provinces (individual provinces or all provinces together), the probability of presence of each province is recalculated for present day conditions except for driver d (from the set of drivers D) for which the end of the century condition is used ($P_n^{future\ for\ dth\ driver\ only}$). The set of driver D can be either all drivers (Fig. 5a,c) or all drivers except SST (Fig. 5b). The relative importance of driver d at a given grid point for the set of N of provinces is computed as follows:

$$RI(d) = \frac{\sum_{n\in N}\left|P_n^{future\ for\ dth\ driver\ only} - P_n^{present}\right|}{\sum_{d\in D}\sum_{n\in N}\left|P_n^{future\ for\ dth\ driver\ only} - P_n^{present}\right|} \quad (4)$$

$RI(d)$ is computed at grid cells where $BC > \frac{1}{6}$ and calculated with either the set of all drivers (Fig. 5a,c) or all drivers except SST (Fig. 5b). When RI(d) is calculated for individual provinces (Fig. 5c and Supplementary Fig. 24d,e), it is computed only at grid cells where $BC > \frac{1}{6}$ and the concerned province is either *dominant* in present day and/or end of century conditions.

## References


51. Jaccard, P. Distribution comparée de la flore alpine dans quelques régions des Alpes occidentales et orientales. *Bull. la Murithienne* (1902).
52. Aumont, O., Ethé, C., Tagliabue, A., Bopp, L. & Gehlen, M. PISCES-v2: An ocean biogeochemical model for carbon and ecosystem studies. *Geosci. Model Dev.* (2015). doi:10.5194/gmd-8-2465-2015
53. Moore, C. M. *et al.* Processes and patterns of oceanic nutrient limitation. *Nature Geoscience* (2013). doi:10.1038/ngeo1765
54. Brun, P., Kiørboe, T., Licandro, P. & Payne, M. R. The predictive skill of species distribution models for plankton in a changing climate. *Glob. Chang. Biol.* (2016). doi:10.1111/gcb.13274
55. Redfield, A. C. On the Proportions of Organic Derivatives in Sea Water and Their Relation to the Composition of Plankton. in *James Johnstone Memorial Volume* 1767–192 (Liverpool Univ. Press, Liverpool, U.K., 1934).
56. Michelangeli, P. A., Vrac, M. & Loukos, H. Probabilistic downscaling approaches: Application to wind cumulative distribution functions. *Geophys. Res. Lett.* (2009). doi:10.1029/2009GL038401
57. Ridgeway, G. gbm: Generalized Boosted Regression Models. *R Packag. version 1.6-3.1* (2010).
58. Breiman, L. & Cutler, A. Breiman and Cutler's random forests for classification and regression. *Packag. 'randomForest'* (2012). doi:10.5244/C.22.54
59. Venables, W. N. & Ripley, B. D. *Modern Applied Statistics with S Fourth edition by*. *World* (2002). doi:10.2307/2685660
60. Wood, S. N. Stable and efficient multiple smoothing parameter estimation for generalized additive models. *J. Am. Stat. Assoc.* (2004). doi:10.1198/016214504000000980
61. Fawcett, T. An introduction to ROC analysis. *Pattern Recognit. Lett.* (2006). doi:10.1016/j.patrec.2005.10.010
62. Biecek, P. DALEX: explainers for complex predictive models. *J. Mach. Learn. Res.* **19**, 1–5 (2018).
63. Jones, M. C. & Cheung, W. W. L. Multi-model ensemble projections of climate

change effects on global marine biodiversity. *ICES J. Mar. Sci.* (2015). doi:10.1093/icesjms/fsu172

64. Vallejos, C. A. Exploring a world of a thousand dimensions. *Nature Biotechnology* (2019). doi:10.1038/s41587-019-0330-9

65. L., K. & P., R. Clustering by means of Medoids. in *Statistical Data Analysis Based on the L1 Norm and Related Methods* (1987).

66. Rousseeuw, P. J. Silhouettes: A graphical aid to the interpretation and validation of cluster analysis. *J. Comput. Appl. Math.* (1987). doi:10.1016/0377-0427(87)90125-7

67. Orsi, A. H., Whitworth, T. & Nowlin, W. D. On the meridional extent and fronts of the Antarctic Circumpolar Current. *Deep. Res. Part I* (1995). doi:10.1016/0967-0637(95)00021-W

68. Hubert, L. & Arabie, P. Comparing partitions. *J. Classif.* (1985). doi:10.1007/BF01908075

69. Somerfield, P. J. Identification of the Bray-Curtis similarity index: Comment on Yoshioka (2008). *Marine Ecology Progress Series* (2008). doi:10.3354/meps07841

70. Bloom, S. Similarity Indices in Community Studies: Potential Pitfalls. *Mar. Ecol. Prog. Ser.* (1981). doi:10.3354/meps005125

71. Watson, R. A. A database of global marine commercial, small-scale, illegal and unreported fisheries catch 1950-2014. *Sci. Data* (2017). doi:10.1038/sdata.2017.39

72. Flanders Marine Institute (2018). Maritime Boundaries Geodatabase: Maritime Boundaries and Exclusive Economic Zones (200NM), version 10. (2018). doi:https://doi.org/10.14284/313.

73. WELCH, B. L. The generalisation of student's problems when several different population variances are involved. *Biometrika* **34**, (1947).

74. Holm, S. A simple sequentially rejective multiple test procedure. *Scand. J. Stat.* **6**, (1979).

75. Mann, H. B. & Whitney, D. R. On a Test of Whether one of Two Random Variables is Stochastically Larger than the Other. *Ann. Math. Stat.* **18**, (1947).

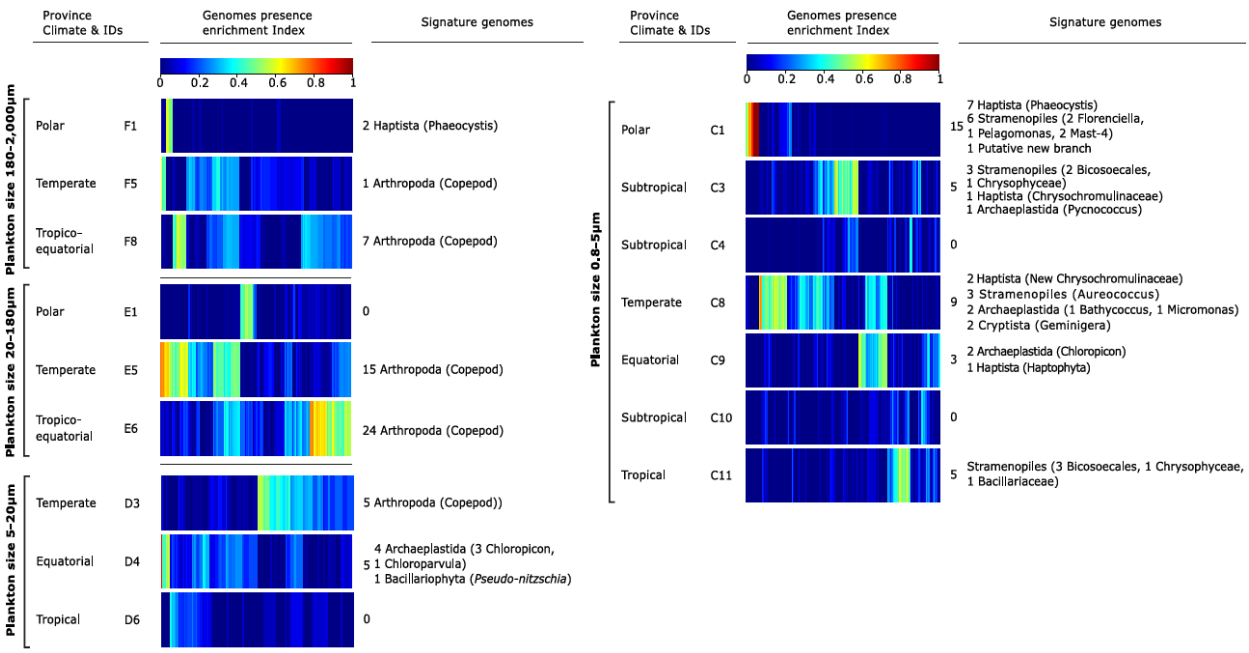


**Fig. 1 | Eukaryotic signature genomes of provinces of eukaryote enriched size classes.** For each plankton size class, indexes of presence enrichment (equation (1)) for 713 genomes of eukaryotic plankton[38] in corresponding provinces are clustered and represented in a color scale. Signature genomes (see *Methods*) are found for almost all provinces, their number and taxonomies are summarized (detailed list in Supplementary Table 6).

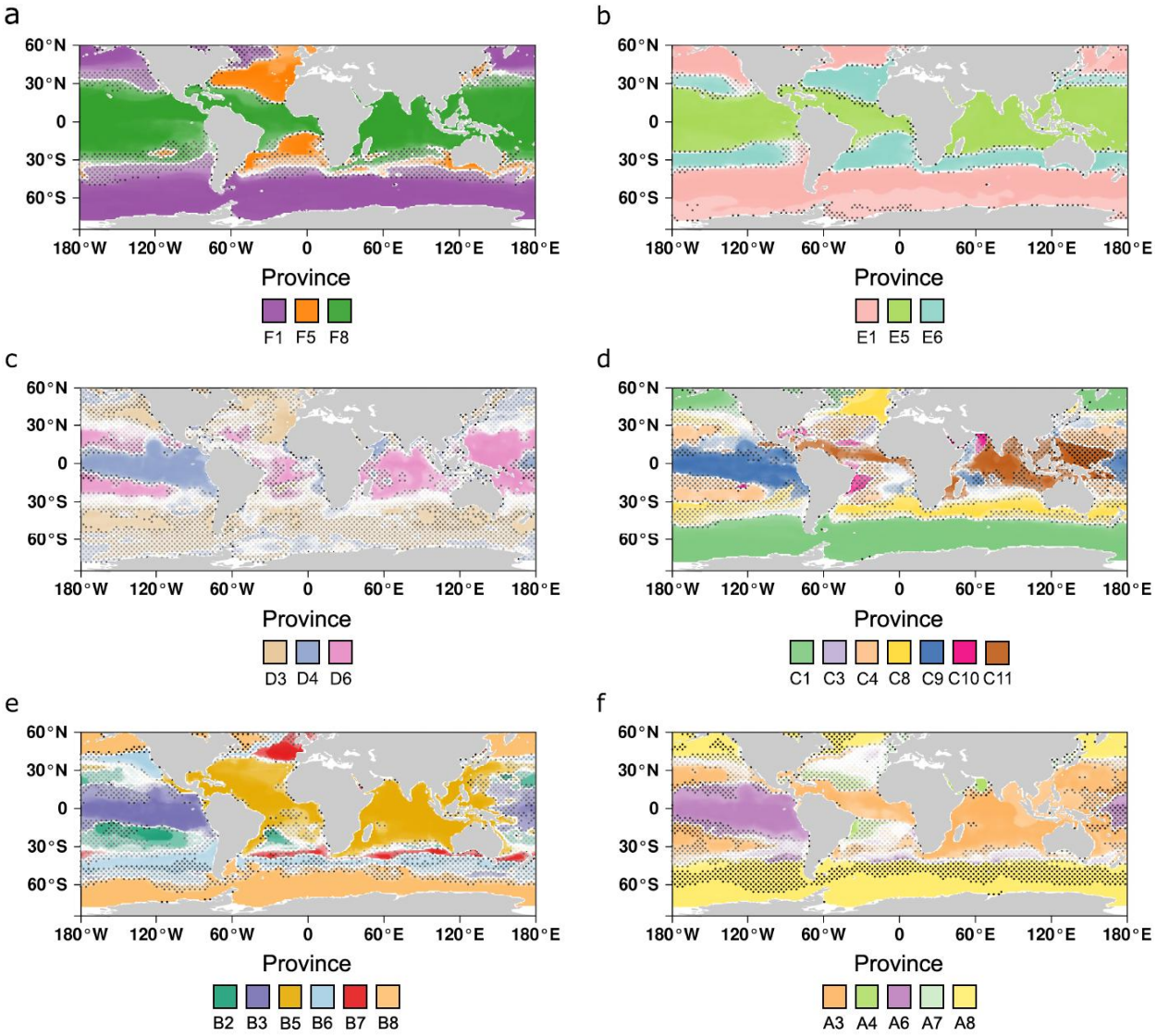


**Fig. 2 | Global biogeographies of size-structured plankton provinces projected on WOA2013 dataset.** (**a**) Metazoans enriched (180-2000 µm) (**b**) Small metazoans enriched (20-180 µm) (**c**) protist enriched (5-20 µm) (**d**) protist enriched (0.8-5 µm) (**e**) Bacteria enriched (0.22-3 µm) (**f**) Viruses enriched (0-0.2 µm). (**a-f**) Dotted areas represent uncertainty areas where the delta of presence probability of the dominant province and an other (from the same size fraction) is inferior to 0.5. Simple biogeographies are observed in large size fractions (>20 µm) with a partitioning in three major oceanic areas: tropico-equatorial, temperate and polar. More complex geographic patterns and patchiness are observed in smaller size fractions with the distinction of pacific equatorial provinces and provinces associated with oligotrophic tropical gyres

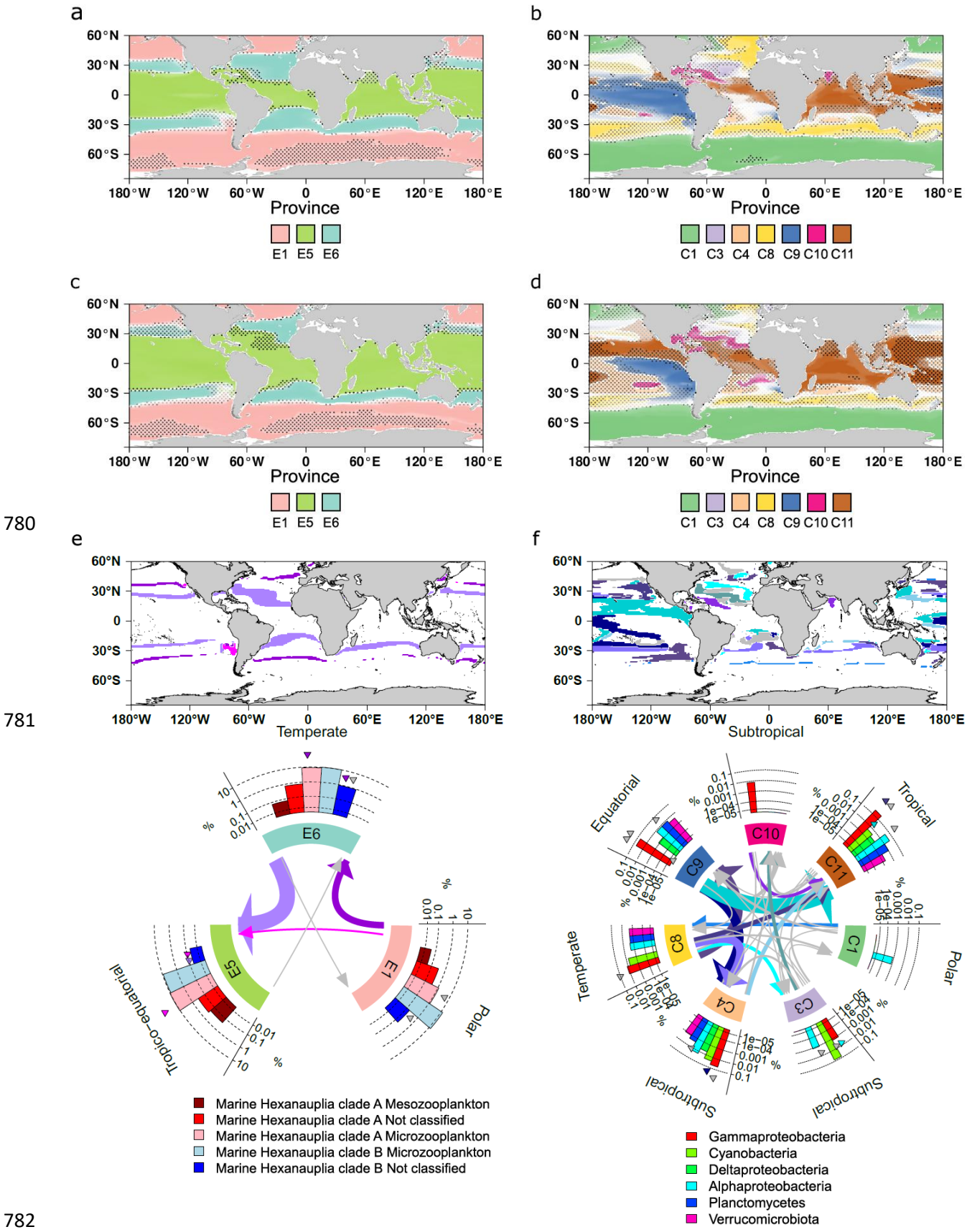

**Fig. 3 | Global biogeographies of the small metazoan enriched size fraction (20-180 µm), the protist enriched size fracton (0.8-5 µm) in (a, b) modeled present day and (c, d) end of the century. Compositional shifts between provinces in (e) marine hexanauplia (180-2000 µm) and (f) diazotrohps (0.8-5 µm).** (**a-d**) The dominant niche *i.e.* the one predicted to have the highest probability of presence is represented at each grid point of the map. The color transparency is the probability of presence of the dominant niche. A simple biogeography is observed for size fraction 180-2000 µm (**a, b**) with a polar niche, a temperate and a tropico-equatorial niche. Biogeography of size fraction 0.8-5 µm is more complex and patchy with several temperate and tropical niches (**c, d**). Biogeography of large size plankton and small size plankton are therefore decoupled. Climate change impacts tropical niches which are expanding towards the poles in both size fractions with a more complex behavior in size fraction 0.8-5 µm (**b** and **d**). Changes in community composition might also happen in areas with out of range projected conditions (*e.g* equator, poles, Supplementary Fig. 12), but here the contemporary province is still the most probable and the climatic label is maintained. (**e-f**) Top: Maps highlighting areas of dominant community shifts in size fraction 20-180 µm (**e**) and 0.8-5 µm (**f**) Bottom: circular plots summarizing significant compositional shifts either in Marine Hexanauplia (copepods) (**f**) or bacterial diazotrophs (**e**): each type of transition is colored differently and accordingly to the one on the map or in grey if they represent less than 2% of the transitions. Barplots represent mean relative abundances in 5 types of Marine Hexanauplia (copepods) (**f**) or main clades of marine diazotrophs (**e**) based on genome abundance in the given province. Arrows represent dominant community shifts pointing towards the end of the century projected province and their widths are proportional to the area of change. Significant compositional changes in a type of genome (*e.g.* cyanobacteria) are represented by triangles of the associated transition color above the corresponding bar (*e.g.* yellowgreen for cyanobacteria) of the barplot of the province projected at the end of the century (which is at the tip of the arrow).

809

| Size fraction (µm) | Present day covered area (%) | End of century covered area (%) | % area with a change of dominant province | Most frequent transition | % | 2nd most frequent transition | % |
|---|---|---|---|---|---|---|---|
| **180-2000** | 74 | 74 | 13 | temperate->tropico-equatorial (F5->F8) | 67 | polar->temperate (F1->F5) | 14 |
| **20-180** | 78 | 77 | 12 | temperate->tropico-equatorial (E6->E5) | 67 | polar->temperate (E1->E6) | 29 |
| **5-20** | 45 | 49 | 22 | temperate -> equatorial (D3->D4) | 47 | equatorial -> tropical (D4->D6) | 25 |
| **0.8-5** | 56 | 59 | 31 | equatorial -> tropical (C9->C11) | 22 | temperate -> equatorial (C8->C9) | 15 |
| **0.22-3** | 60 | 61 | 15 | temperate-> tropical (B7->B5) | 22 | polar -> temperate (B8->B6) | 16 |
| **0-0.2** | 64 | 66 | 16 | equatorial -> tropical (A6->A3) | 32 | temperate -> equatorial (A8->A6) | 31 |
| **Total** | | | **60** | | | | |

810 **Table 1 | Global statistics of covered areas and province changes and transitions.** From
811 12% to 31% of the total covered area is estimated to be replaced by a different province at the
812 end of the century compared to present day depending on the size fraction. In total, considering
813 all size fractions this represents 60% of the total covered area with at least one predicted
814 change of dominant province across the six size fractions.

815

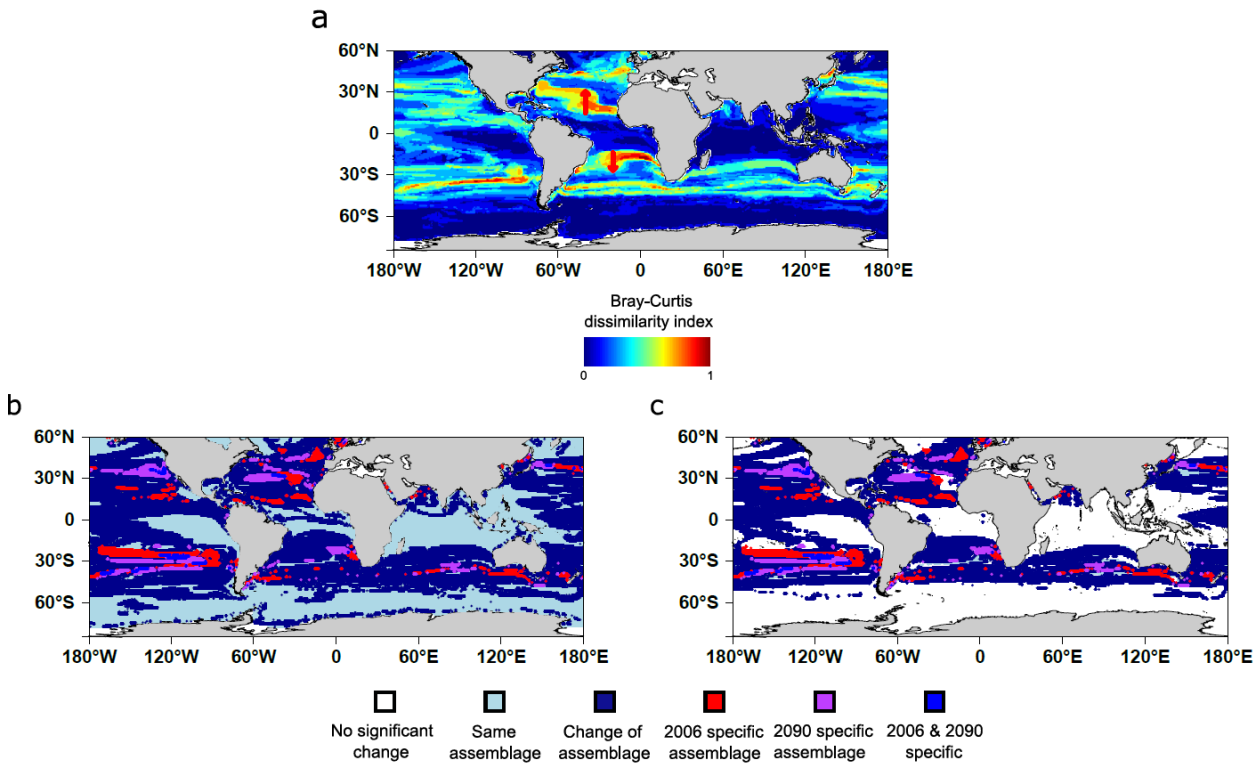


816 **Fig. 4 | (a) Bray-Curtis dissimilarity index map comparing present day with end of the**
817 **century projections of dominant provinces. Maps of trans-kingdom assemblage**
818 **reorganization of dominant provinces (b) and with a criterion of significance (c).** (**a**) Bray-
819 Curtis dissimilarity index (equation (3)) is calculated by integrating all the dominant provinces
820 presence probabilities over the six size fraction. Most important changes appear in subtropical,
821 temperate and subpolar regions. These changes are due to the displacement of tropical and
822 temperate provinces towards the pole but also the geographical decoupling between large and
823 small size plankton. The mean change in niche dissimilarity index is 0.25. (**b**) An assemblage is
824 the combined projected presence of the dominant province of each size class. Assemblage
825 reorganization (present day versus end of the century) is either mapped on all considered
826 oceans or with a criterion on the Bray-Curtis dissimilarity index (BC>1/6, see *Materials and*
827 *Methods*) (**c**). Depending on the criterion from 60.1% (**b**, dark blue) to 48.7% (**c**, dark blue) of
828 the oceanic area is projected to change of assemblage. New assemblages are expected to
829 appear in 2090 (purple+blue) whereas some 2006 specific assemblages are projected to
830 disappear (red+blue). New assemblages as well as lost assemblages are mostly found in
831 temperate, subtropical and tropical regions where most of the rearrangements are projected.

832

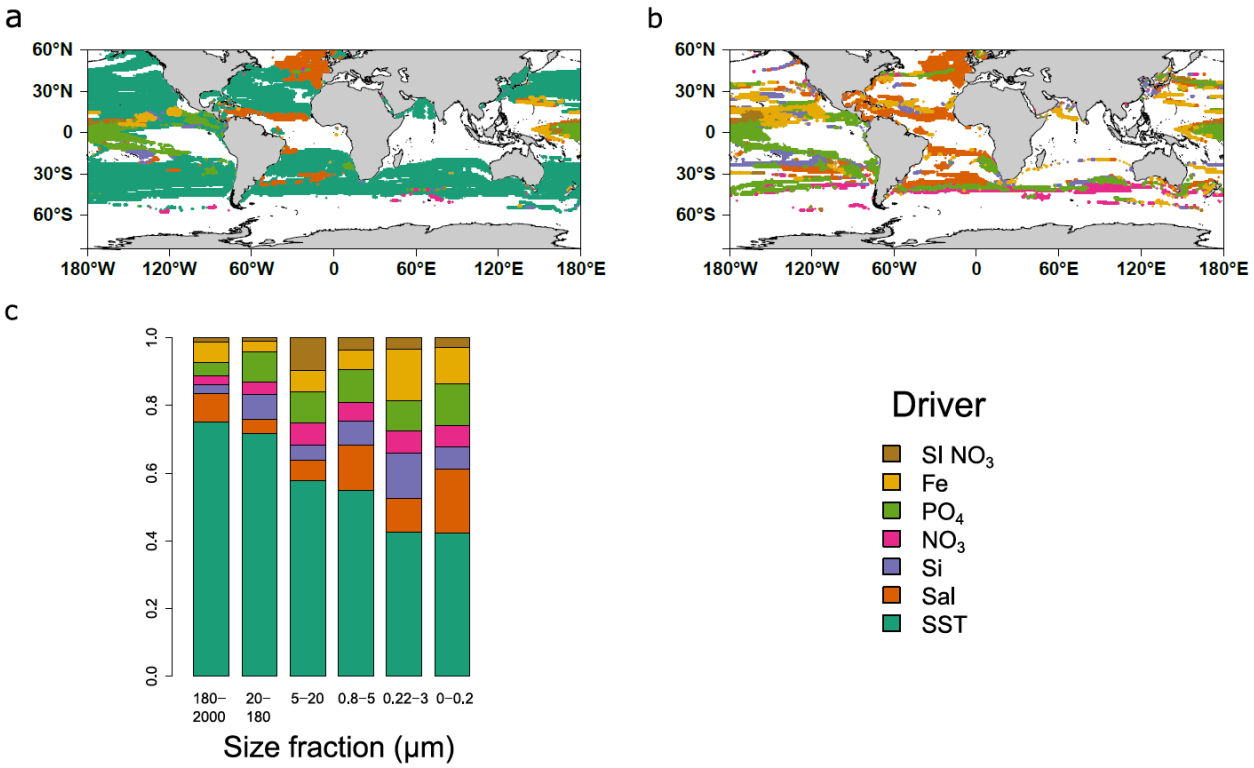


**Fig. 5 | Map of most impacting drivers on dominant province changes (a), most impacting driver without considering temperature change (b) and relative importance of the drivers in the different size fractions (c).** (**a**) Temperature appears as the top impacting driver on the majority of the projected ocean with a significant change of province (Fig. 4). (**b**) Salinity and dissolved phosphate are found to be the second and third drivers of province reorganization notably at tropical and subpolar latitudes. Note the importance of nitrate at temperate southern latitudes. (**c**) Temperature is found to be the most important driver for all size classes but has a more important impact in large size classes (>20 µm). Nutrients have on average a relatively more important impact in small size classes in driving province reorganization.

## Supplementary information 1 | Niche models of genomic provinces

To compute and test the validity of realized environmental niches, we train four machine learning techniques to probabilistically associate genomic provinces with environmental data: sea surface temperature, salinity, three macronutrients (dissolved silica, nitrate and phosphate), one micronutrient (dissolved iron) plus a seasonality index of nitrate. The four machine learning techniques are Gradient Boosting Machine (gbm)[1], Random Forest (rf)[2], fully connected Neural Networks (nn)[3] and Generalized Additive Models (gam)[4]. Following a cross-validation framework, a valid environmental niche is obtained for 27 out of 38 initial provinces (71%) comforting their definition and covering 529 samples out of 595 (89%, Supplementary Fig. 2). Rejected provinces contain relatively few stations (mean of 6 ± 2.6 versus 19 ± 15.3 for valid provinces, p-value<$10^{-3}$ Wilcoxon test[5]). For spatial and temporal extrapolations of the provinces presented below, we use the ensemble model approach[6] that considers mean predictions of machine learning techniques.

## Supplementary information 2 | Integrated biogeographies using the PHATE algorithm

We use the PHATE dimension reduction algorithm[7] to combine all provinces for all size classes into a single consensus biogeography revealing 4 or 7 robust clusters (Supplementary Fig. 5, *methods*). The 4 cluster consensus biogeography is mainly latitudinally organized distinguishing polar, subpolar, temperate and tropico-equatorial regions. The 7 cluster consensus biogeography distinguishes the equatorial pacific upwelling biome and three subpolar biomes that most likely reflect the chemico-physical structuring of the Southern Ocean and known polar fronts[8] (red lines Fig. 2h). However, learning data are scarcer south of 60°S so these extrapolations need to be taken with caution.

PHATE is also used for modeled projections into two comparable consensus maps, one for present day and one for the end of the century (Supplementary Fig. 17). Some particularly visible patterns of geographical reorganization are common to several or even all size fractions and visible when comparing the two consensus maps (Supplementary Fig. 17 compared to Fig. 3a-d and Supplementary Fig. 14). For

874 example, the tropico-equatorial and tropical provinces expand in all size fractions and
875 the provinces including the pacific equatorial upwelling shrink for size fractions smaller
876 than 20 µm.
877
878 **Supplementary information 3 | Comparison of the biogeographies with existing**
879 **partitions of the oceans**
880 Previous ocean partitioning either in biomes[9–11] or biogeochemical provinces
881 (BGCPs)[9,10] are based on physico-biogeochemical characteristics including SST[9–11],
882 chlorophyll *a*[9–11], salinity[9–11], bathymetry[9,10], mixed layer depth[11] or ice fraction[11].
883 Considering three of these partitions as examples we notice differences with our
884 partitions (Supplementary Fig. 8-9) for example in terms of the number of regions in the
885 considered oceans (56 for 2013 Reygondeau et al. BGCPs[10], 17 for Fay and
886 McKingley[11]) and their structure (the coastal biome for 2013 Reygondeau et al.
887 biomes[10]). Numerical comparison of our partitions with others (*Methods*) reveals low
888 similarity between them, the highest being with Reygondeau biomes (Supplementary
889 Figs. 8-10). However, biomes and BGCP frontiers closely match our province frontiers
890 in many cases. Near the frontiers, *dominant* provinces have smaller probabilities in
891 agreement with smooth transitions instead of sharp boundaries as already proposed[9]
892 and with a seasonal variability of the frontiers[10] (Supplementary Fig. 8). Some of these
893 transitions are very large and match entire BGCPs, for example in subtropical North
894 Atlantic and subpolar areas where high annual variations are well known[10].
895
896 **Supplementary information 4 | Expansion and shrinkage of provinces in response**
897 **to climate change**
898 To quantify patterns of expansion or shrinkage of the provinces, we calculate the
899 surface covered by the *dominant* provinces weighted by probabilities of presence
900 (Supplementary Fig. 18, Supplementary Table 2). In this way, *dominant* provinces are
901 defined on 100% of the surface ocean (327 million $km^2$) but their presence probabilities
902 correspond to the equivalent of 45 to 74% (due to sampling variability and niche
903 overlaps) of the surface ocean depending on the plankton size fraction (Table 1).
904 Overall, our results indicate expansions of the surface of tropical and tropico-equatorial

905 provinces but in very different ways depending on the size fractions of organisms. The
906 surface area of temperate provinces is ~22 million $km^2$ on average (from 10 $Mkm^2$ for
907 0-0.2 µm to 49 $Mkm^2$ for 20-180 µm) and should decrease by 36% on average (from -20
908 % for 5-20 µm up to -54% for 0.8-5 µm, -12 million $km^2$ on average, +6% for 0.22-3
909 µm). Tropical provinces cover ~118 million $km^2$ on average (from 86 $Mkm^2$ for 0.8-5 µm
910 up to 169 $Mkm^2$ for 180-2000 µm) and their coverage should increase by 32% on
911 average (from +13% for 0-0.2 µm up to +75% for 0.8-5 µm, +25 million $km^2$ on average)
912 (Supplementary Fig. 18 and Supplementary Table 2).

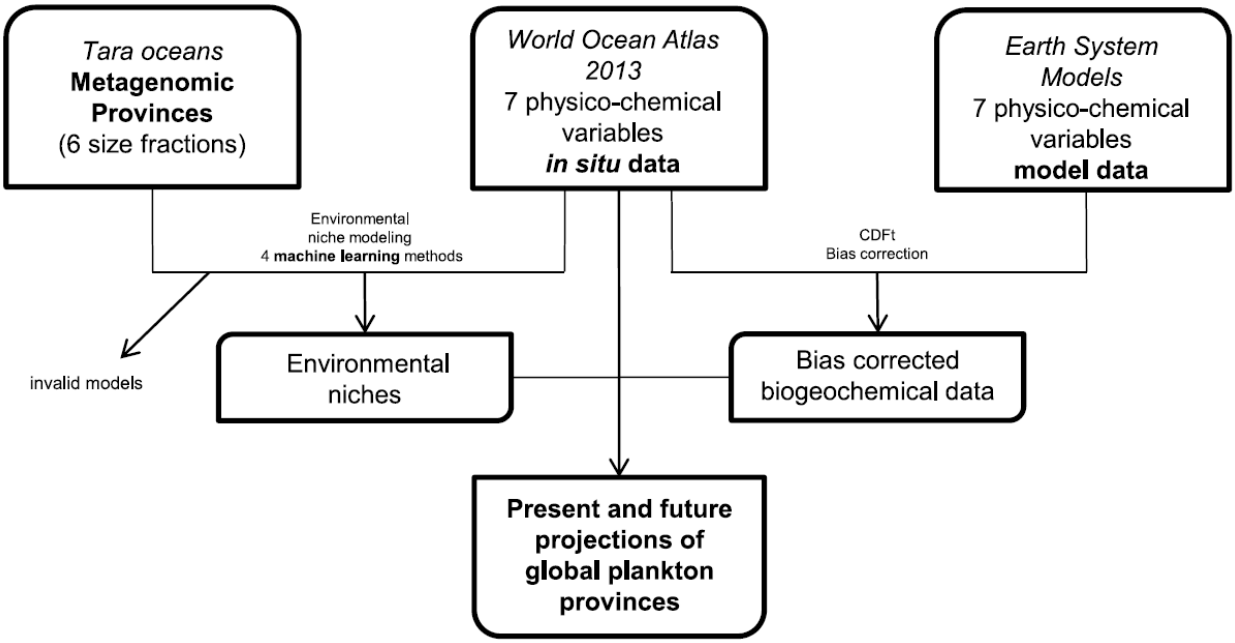


**Supplementary Fig. 1 | Study pipeline.** Metagenomic data from the 2009-2013 *Tara Oceans* expedition and *in situ* measurements of physicochemical variables (*World Ocean Atlas 2013*, WOA13)[12] are combined to define environmental niches at the plankton community level across 6 size fractions of the plankton realm. Bias corrected outputs from a mean model of 6 Earth System Models[13–18] and WOA13 data are then used to project global plankton provinces for present day conditions and end of the century conditions under a high warming scenario (RCP8.5)[19]. Physico-chemical variables are Sea Surface Temperature (SST), Salinity (Sal), Dissolved silica (Si), Nitrate ($NO_3$), Phosphate (PO4), Iron (Fe) and a seasonality index of nitrate (SI $NO_3$).

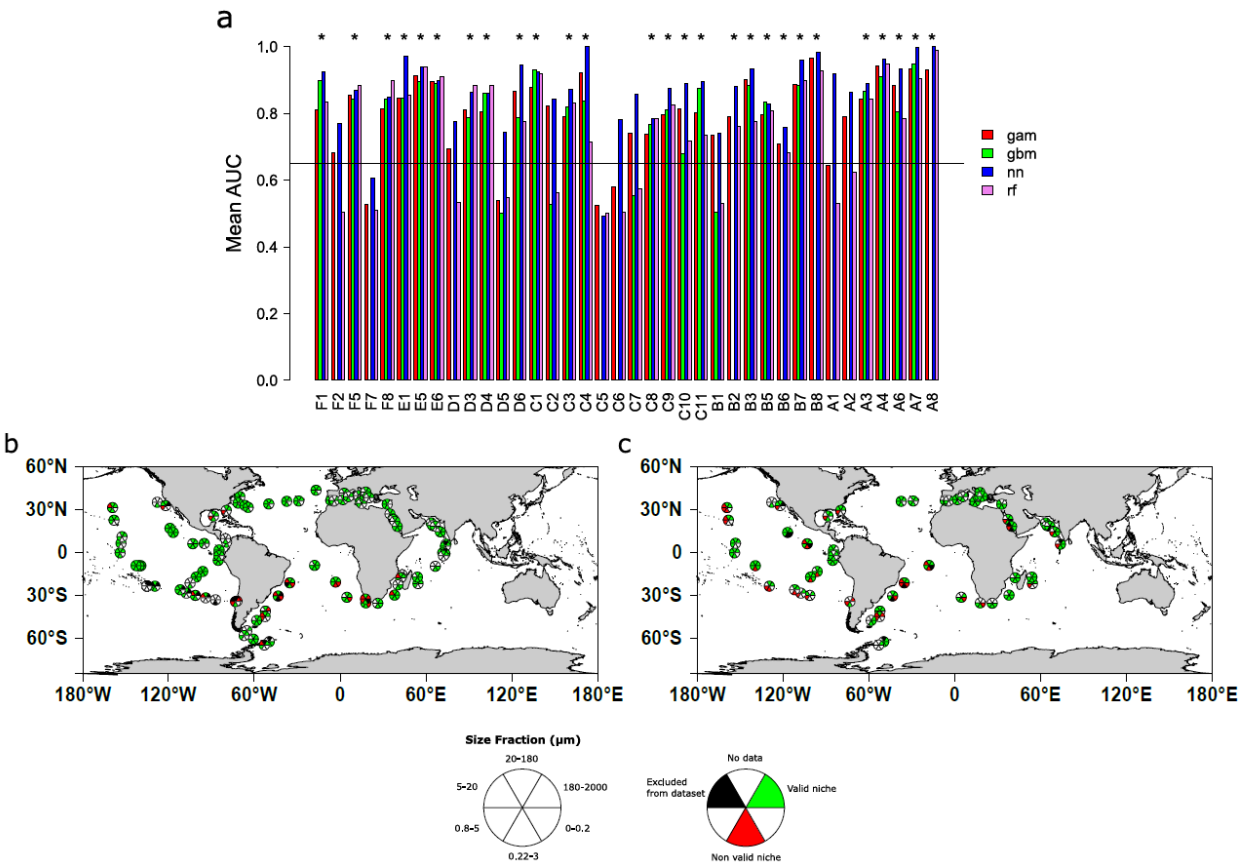


**Supplementary Fig. 2 | (a) Barplot of mean AUC over a random 30-fold cross validation process of the 38 initial metagenomic provinces. (b,c) Map of validated and non validated stations across the six size fractions in surface samples (b) and DCM samples (c).** (**a**) Mean AUC (Area Under the receiver operating Characteristic)[20] is plotted for the best hyperparameter combination of the 4 machine learning techniques used for each of the 38 metagenomic provinces. General Additive Models[4] (gam) are shown in red (no optimization), Gradient Boosting Machines[1] (gbm) in green, fully connected Neural Networks[3] (nn) in blue and Random Forest[2] models in purple (rf). A star for valid models is drawn at the top of each considered valid model. A model is validated when at least 3 out of the four models have a mean AUC superior to 0.65. A valid model is found for 27 out of 38 initial provinces. Out of the 27 validated models 4 are not valid for the gbm method. (b-c) For each Tara sample present in the dataset at surface (b) or Deep Chlorophyll Maximum (DCM) (c) and for each size fraction, the filter (one size fraction at one location and one depth) belongs either to a validated niche (green), a non validated niche (red), an excluded filter (sea *Materials & Methods*) (black) or no data is available (white). Non validated niches represent only 11% of filters present in the dataset (66 out of 595).

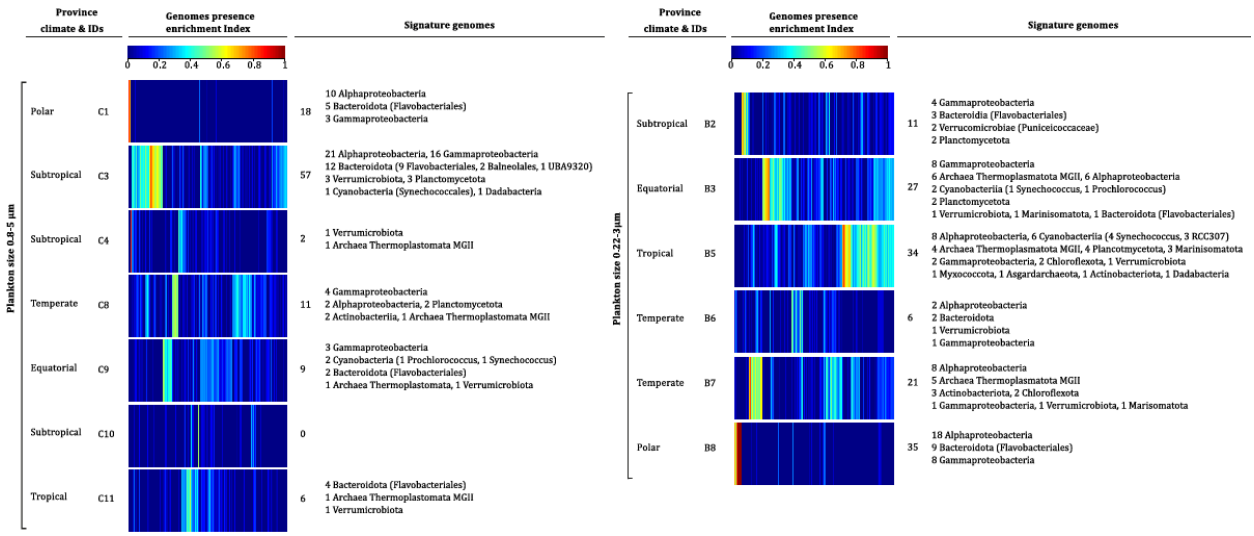


**Supplementary Fig. 3 | Prokaryotic signature genomes of provinces of the prokaryote (0.22-3 µm) and protist (0.8-5 µm) enriched size classes.** Indexes of presence enrichment[21] for 1888 genomes of prokaryotic plankton[22] in corresponding provinces are clustered and represented in a color scale. Signature genomes (see *Methods*) are found for almost all provinces, their number and taxonomies are summarized (detailed list in Supplementary Table 6).

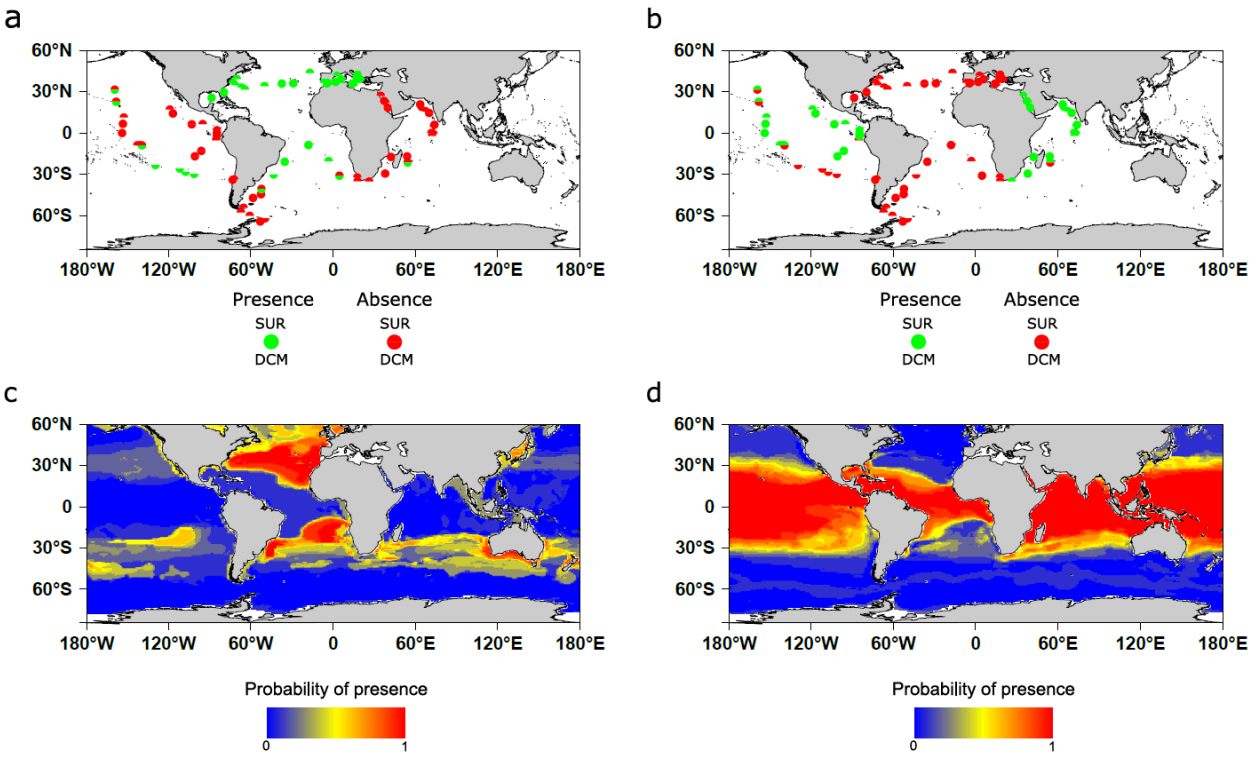


946 **Supplementary Fig. 4 | Sampling and projection maps on WOA13 climatological data of**
947 **two example provinces from size fraction 180-2000 µm.** (**a**) Sampling map of province F5.
948 (**b**) Province F8. (**c**) Projection map of province F5 on WOA13[12]. (**d**) Province F8. Qualitatively,
949 projection maps are coherent with sampling maps of the two provinces with the highest
950 probability of presence projected in the sampling regions. Other presence zones are also
951 predicted by the projection. Sampling of these zones might be interesting to confirm our
952 approach and projections such as South of Australia where a high probability of presence for
953 province F5 is predicted.

954

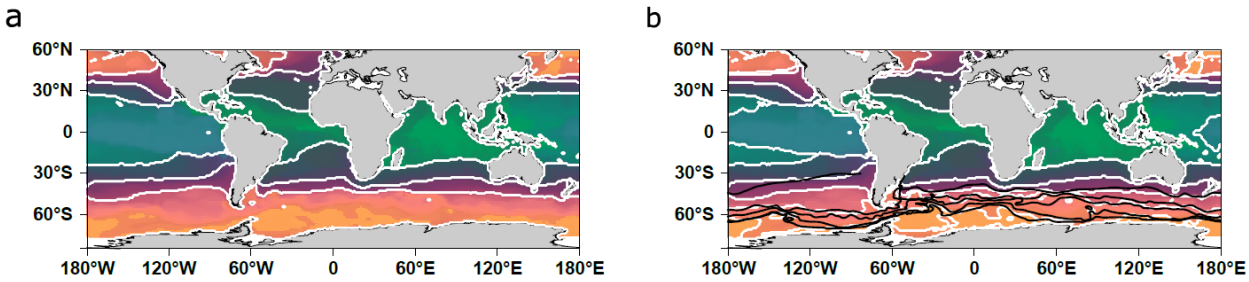


**Supplementary Fig. 5 | Present day combined size class biogeographies using the PHATE algorithm on WOA13 dataset.** (**a**) Combined size class biogeography using PHATE algorithm[7] partitioned in 4 clusters. Each grid point is associated to a color depending on its PHATE coordinates (using three axes). Each coordinate is respectively assigned to a given degree of color between 0 and 255 according to equation 2 (either red green or blue depending on the axis).(**b**) Combined size class biogeography using PHATE algorithm partitioned in 7 clusters overlaid with Antarctic Circumpolar Current boundaries (black). Colors are the same as in (**a**).

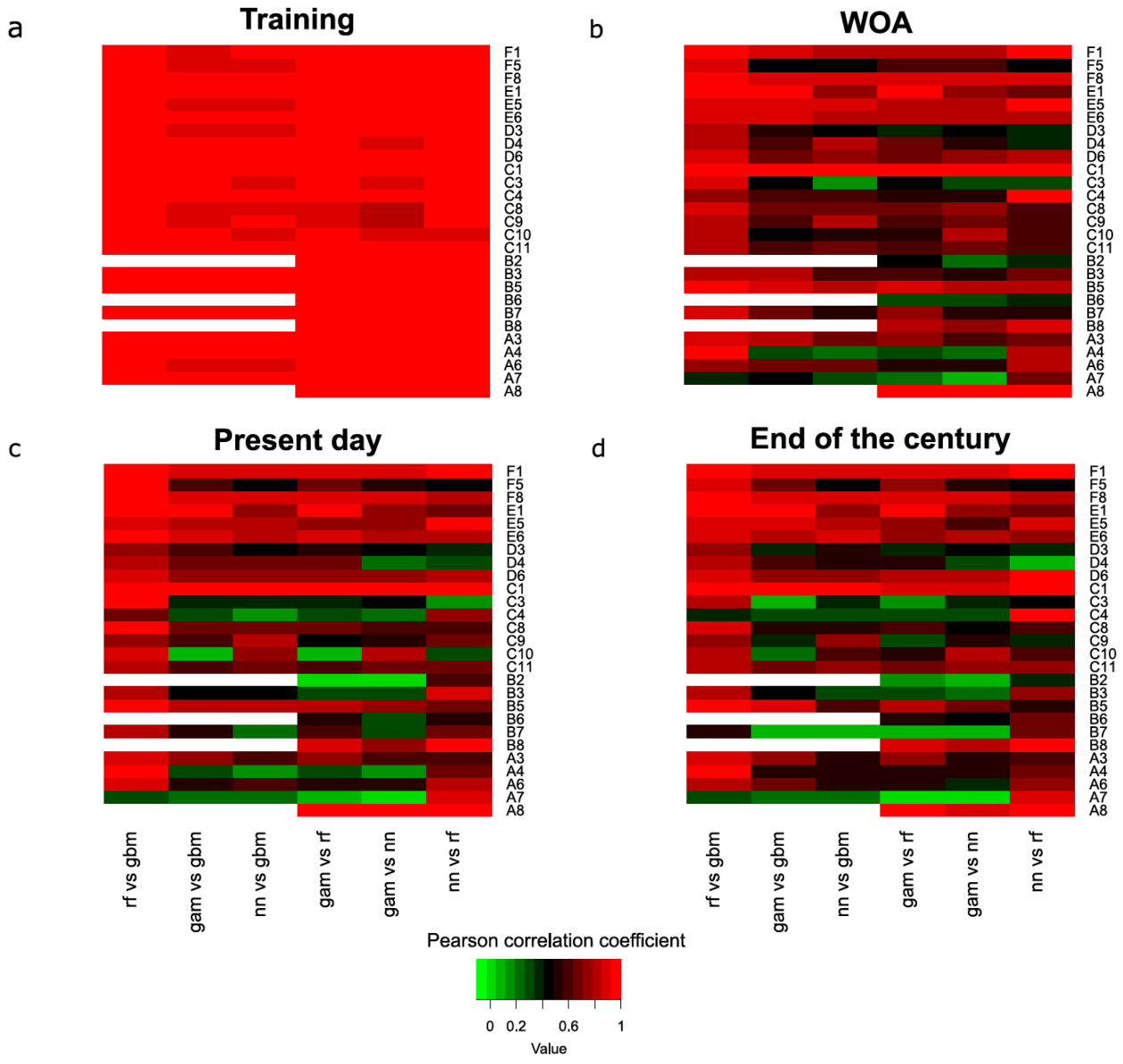


964
965 **Supplementary Fig. 6 | Pairwise Pearson correlation coefficient heat maps between**
966 **outputs of the 4 machine learning models.** rf: Random Forest, gbm: gradient boosting
967 machines, gam: general additive models, nn: neural networks. The rows are the provinces of
968 the different size fractions. The columns are the pairwise comparisons of each machine learning
969 technique. (a) Training set outputs. (b) WOA13 average data projections outputs (except for
970 Iron, PISCES-v2[23] is used). (c) Present day data projection outputs (bias corrected mean model
971 of 6 Earth System Models). (d) End of the century projection outputs. On the training set,
972 models are in agreement with most of the correlation coefficients superior to 0.9. A drop in
973 correlation is observed for modeled data (c, d) especially in small size fractions. This shows
974 modeled data are more distant from the training set than WOA data. Random Forest and

975 Gradient Boosting Machine are in very good agreement (first columns) which could be expected
976 as they are both based on multiple decision trees.

977

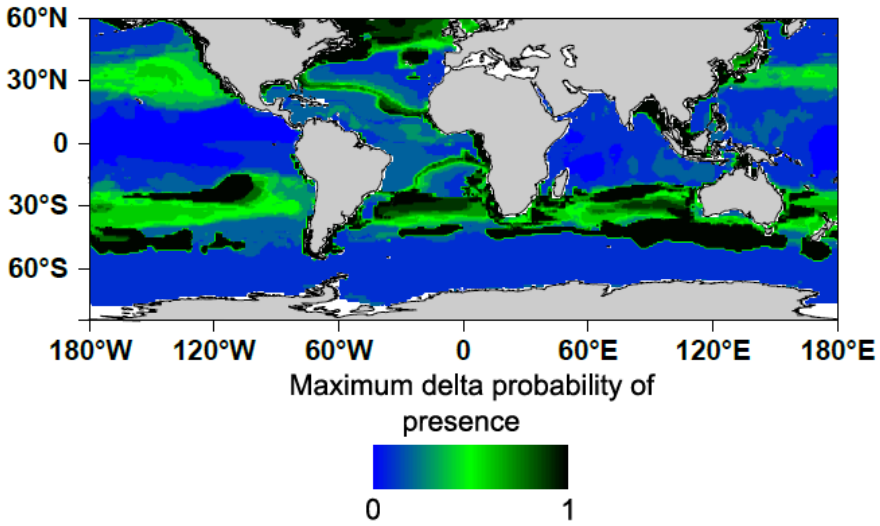


978 **Supplementary Fig. 7 | Probability range map (WOA data) of province F5 of size fraction**
979 **180-2000 µm.** At each point of the grid, the maximum delta probability of presence between the
980 4 machine learning projections is calculated. In black are the zones where two models
981 completely disagree: one model predicts presence with certainty whereas the other predicts
982 absence with certainty. Disagreement appears mostly in uncertain presence areas
983 (Supplementary Fig. 4c) whereas models are generally in good agreement in absence areas
984 (blue zones).

985

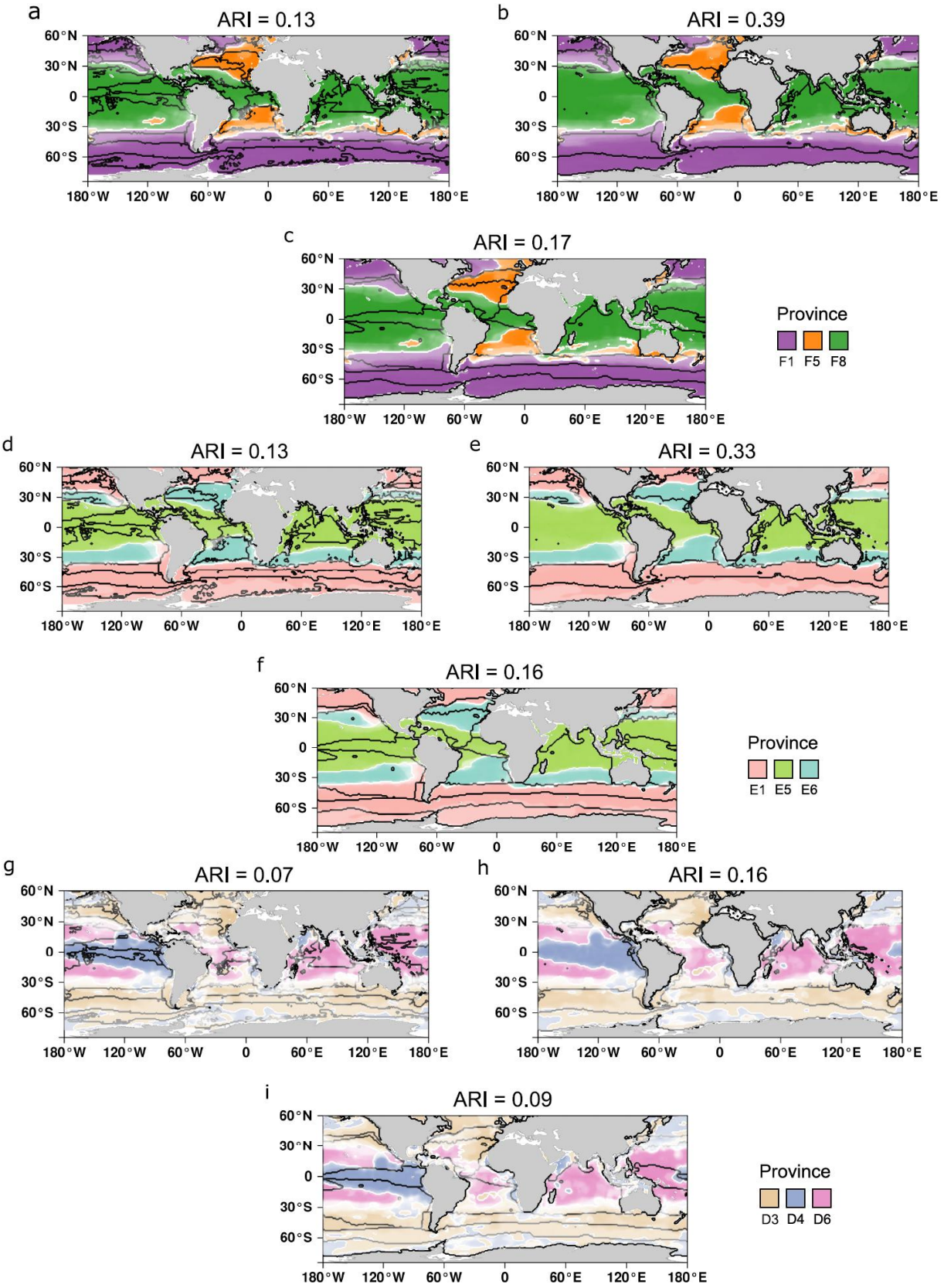


986

987

988

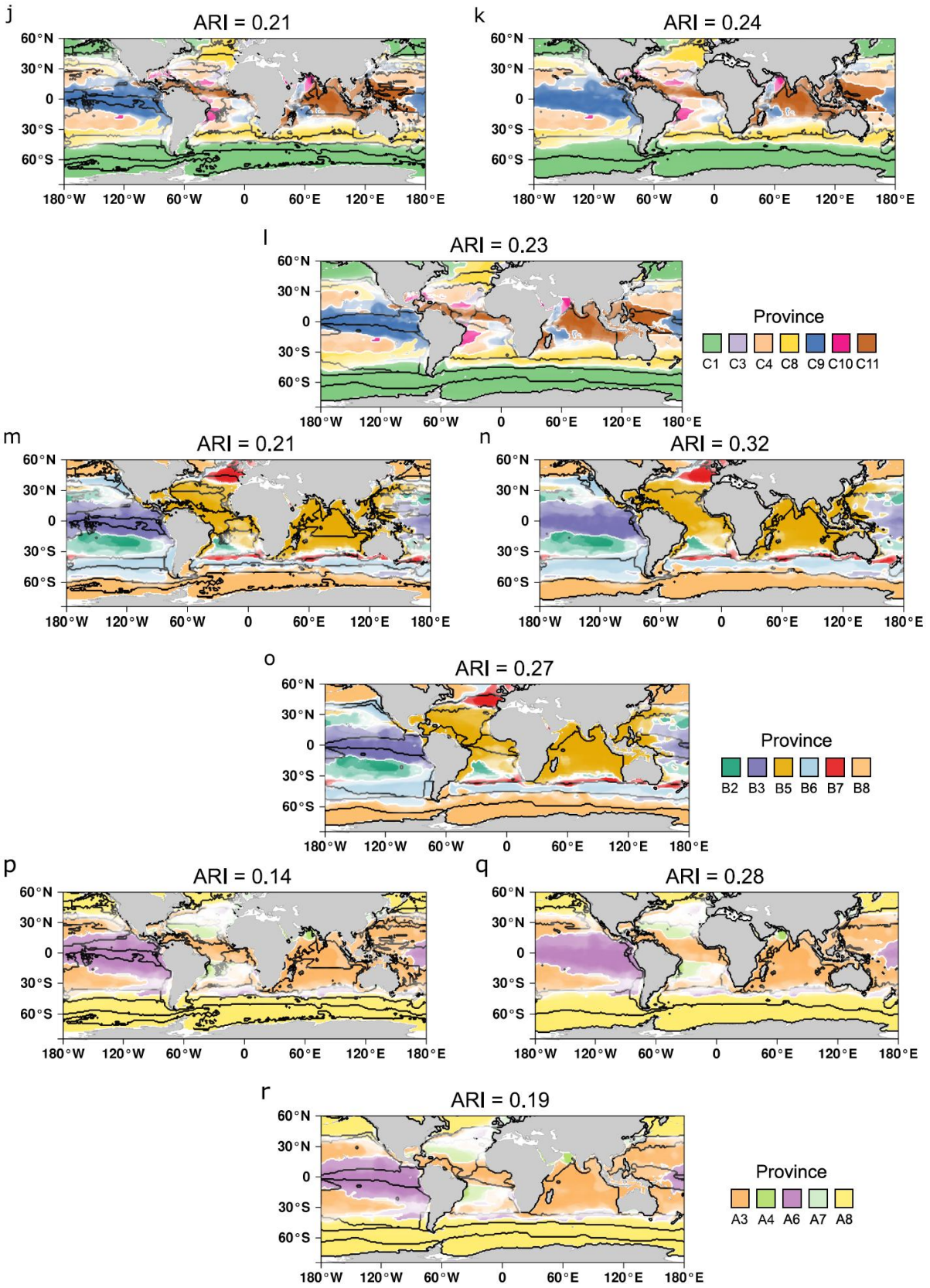


**Supplementary Fig. 8 | Three existing oceanic partitions overlaid on top of plankton**

**provinces for the six fractions and combined size fractions.** The three oceanic partitions are Reygondeau et al. Biogeochemical Provinces (BGCP)[10]; Reygondeau et al. Biomes[10]; Fay and McKingley Biomes[11]. Each partitioning mask is overlaid in the above order on top of plankton provinces for the six size fractions. (**a-c**) 180-2000 µm (**d-f**) 20-180 µm (**g-i**) 5-20 µm (**j-l**) 0.8-5 µm(**m-o**) 0.22-3 µm and (**p-r**) 0-0.2 µm. Above all maps, the adjusted rand index (ARI, an index used to compare partitions), for the comparision of mapped biogeographies with the black line mask is shown.

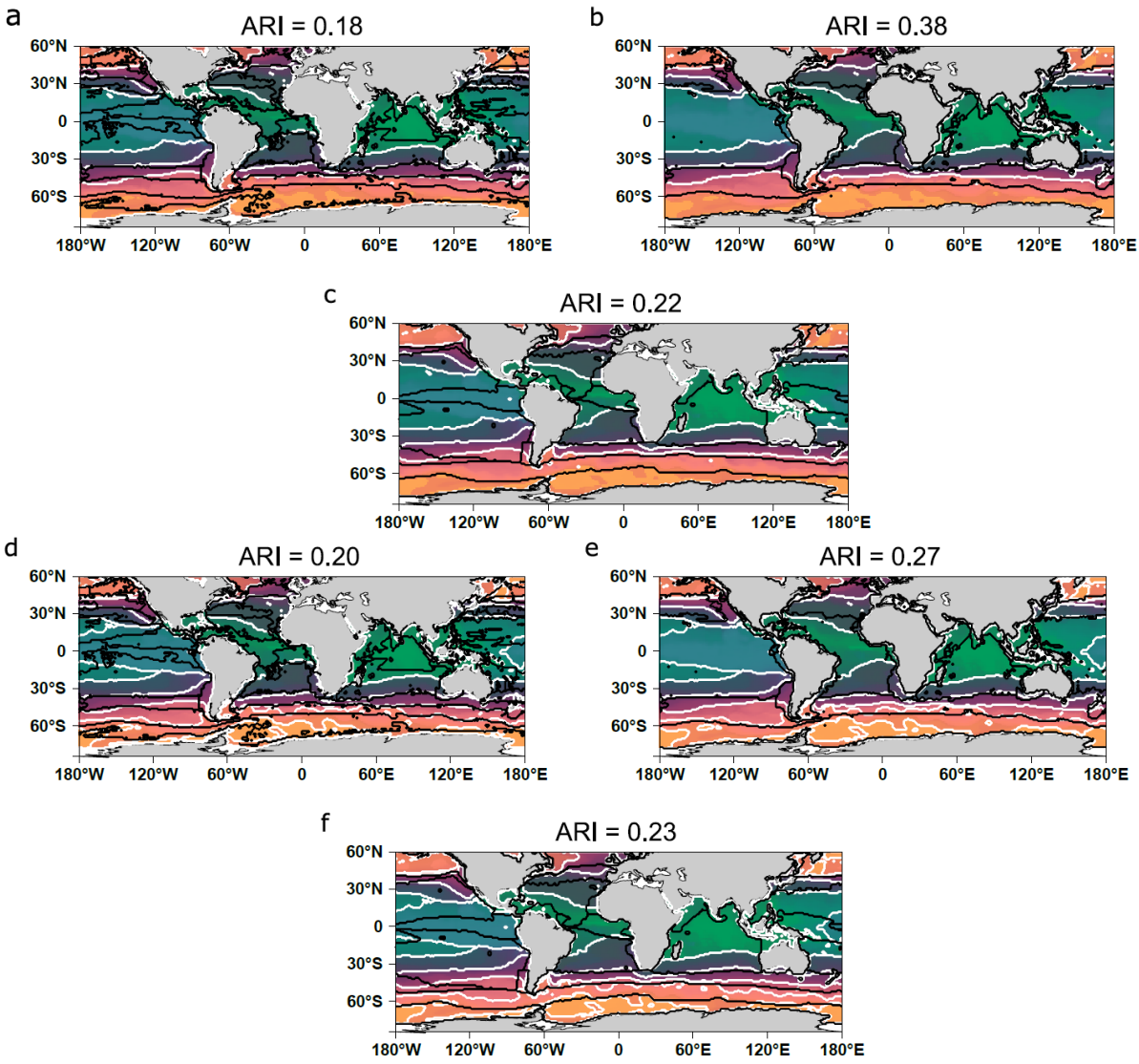


**Supplementary Fig. 9 | Three existing oceanic partitions overlaid on top of plankton provinces for the combined size fractions.** The three oceanic partitions are Reygondeau et al.[10] Biogeochemical Provinces (BGCP); Reygondeau et al. Biomes[10]; Fay and McKingley Biomes[11]. Each partitioning mask is overlaid in the above order on top of size fraction plankton provinces combined by the PHATE algorithm in (**a-c**) 4 clusters and (**d-f**) 7 clusters. Each grid point is associated with a color depending on its PHATE coordinates (using three axes). Each coordinate is respectively assigned to a given degree of color between 0 and 255 according to equation 2 (either red green or blue depending on the axis).

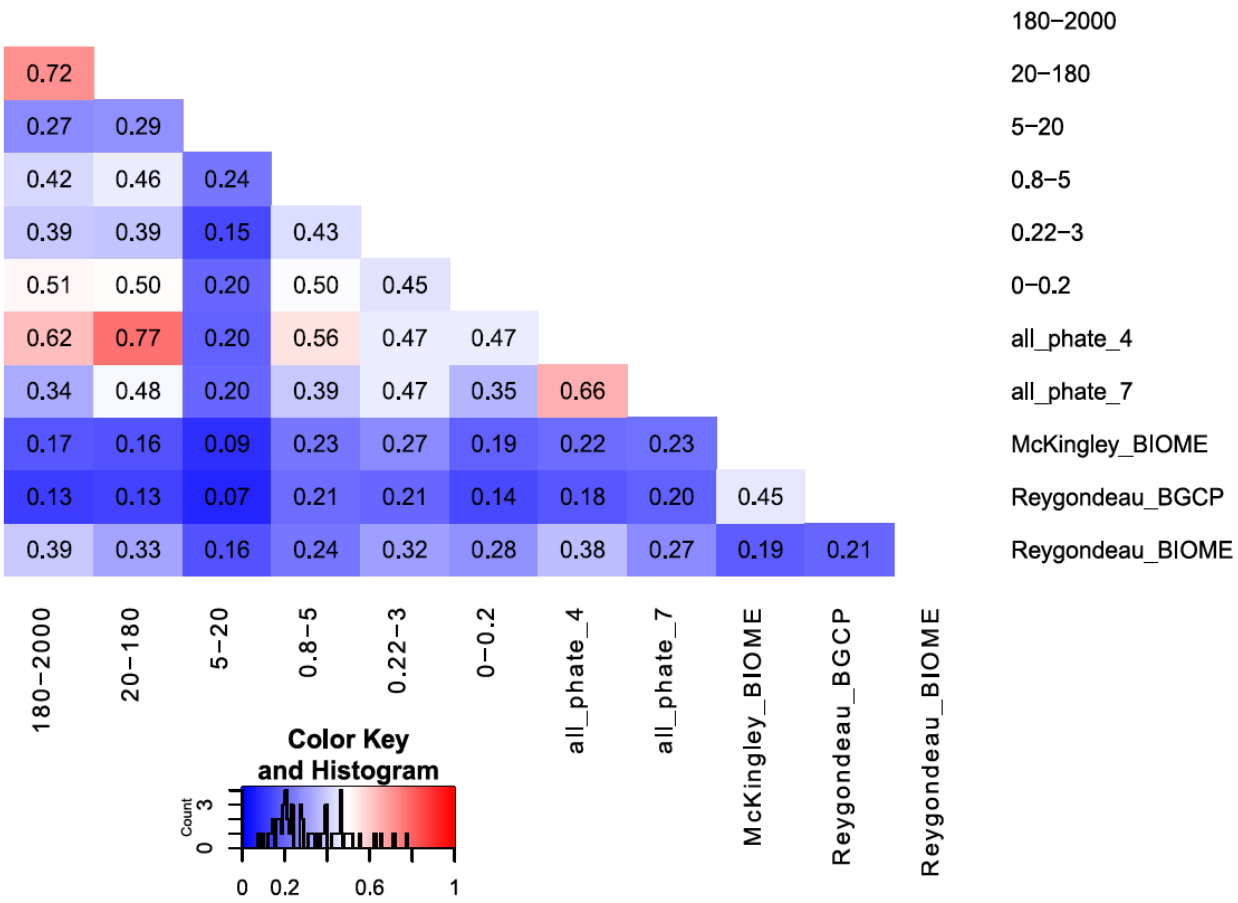


**Supplementary Fig. 10 | Pairwise comparisons of ocean partitions based on plankton provinces and existing biogeochemical partitions.** The three oceanic partitions are Reygondeau et al.[10] Biogeochemical Provinces (BGCP); Reygondeau et al. Biomes[10]; Fay and McKingley Biomes[11].

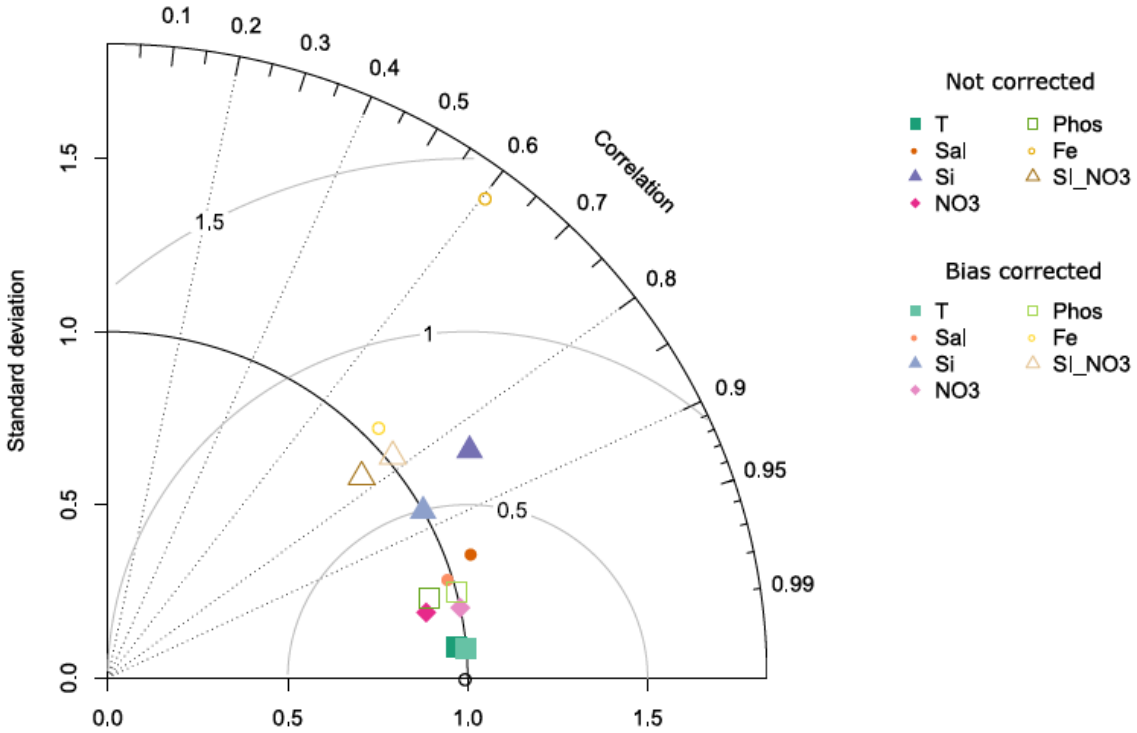


**Supplementary Fig. 11 | Taylor diagram exhibiting statistical comparison of WOA 2013 observations and present day ESM model mean of the different drivers.** Each variable is centered and scaled according to the mean and standard deviation of the observed variable (black circle point at standard deviation 1 on the x-axis). Dark color points are the ESM model mean without Cumulative Distribution Function transform (CDFt[24]) bias correction. They are to be compared with light color points for which the bias correction is performed. Overall, good spatial correlations are found between the model mean and the observations. CDFt bias correction performs well by bringing standard deviations of the model to the observed standard deviations without decreasing correlations.

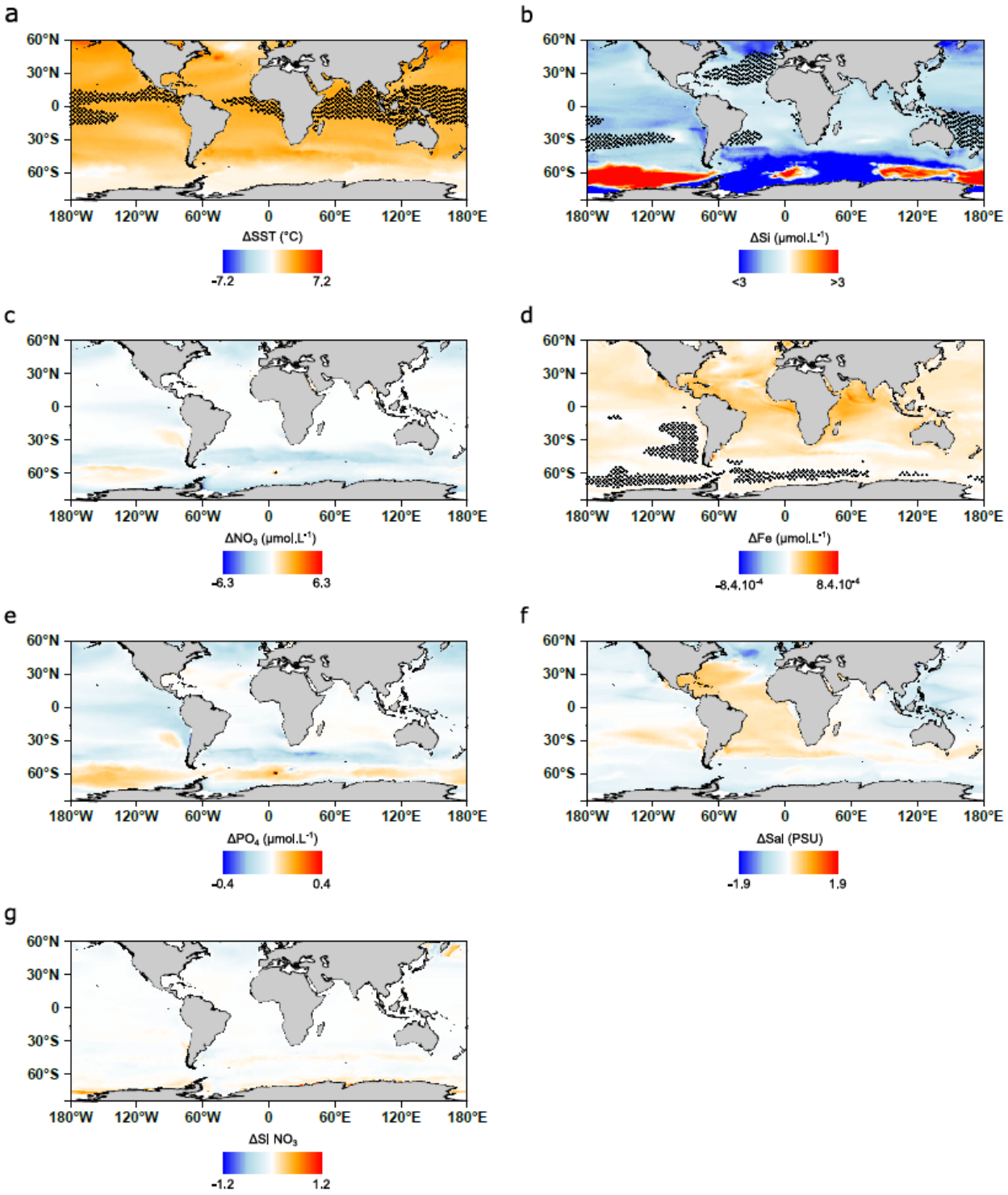


**Supplementary Fig. 12 | Differences in drivers' intensity (2090/99-2006/15) in the bias corrected ESM model-mean under RCP8.5.** (**a**) Sea Surface Temperature (SST). (**b**) Dissolved silica. (**c**) Nitrate. (**d**) Iron. (**e**) Phosphate. (**f**) Salinity (Sal). (**g**) Seasonality Index of Nitrate (SI $NO_3$). Note that the scale for dissolved silica variations is restricted to visualize small variations. Regions for which out of range values (*i.e.* inferior to the minimum or superior to the

1033 maximum found in 2006-15) are reached at the end of the century are highlighted with small
1034 stars reflecting high uncertainty zones for machine learning approaches.

1035

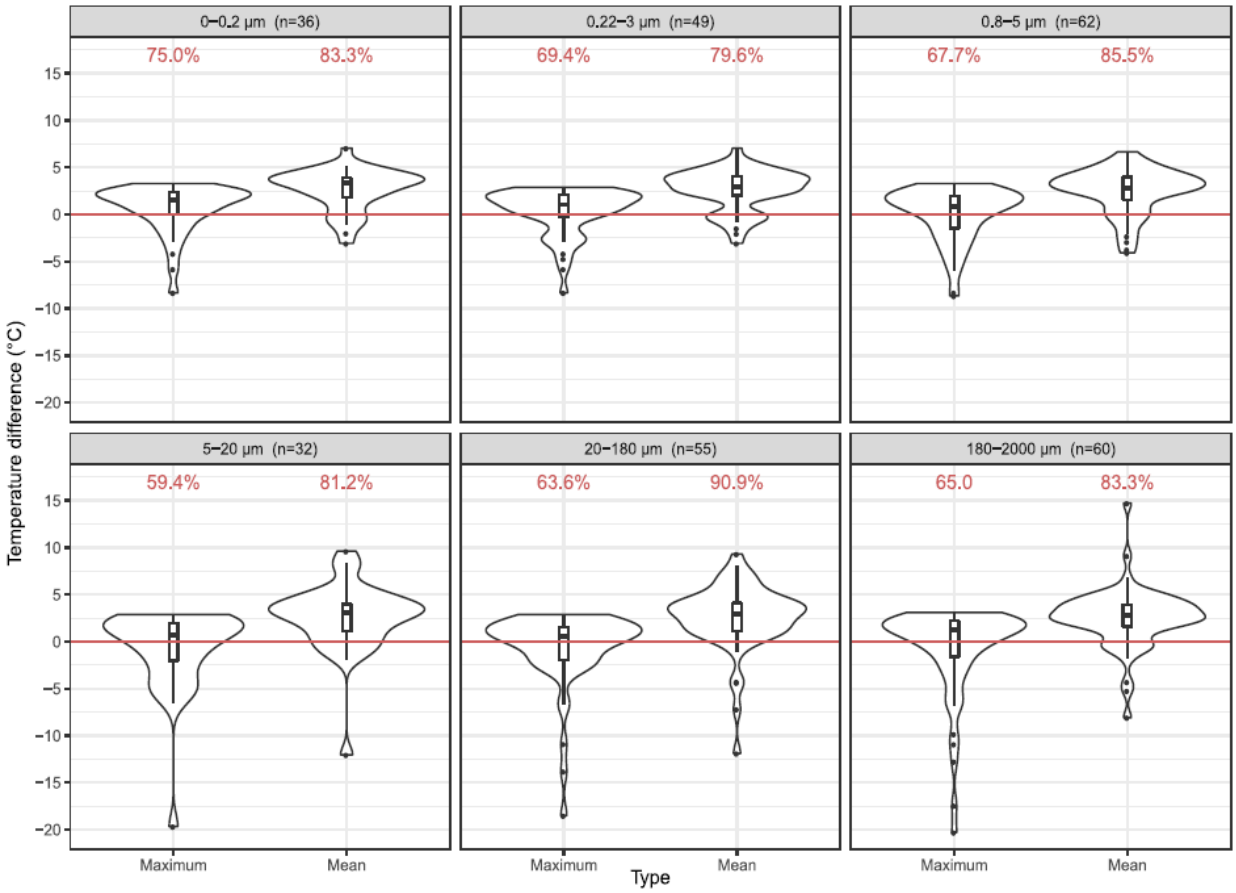


**Supplementary Fig. 13 | Distribution of deltas between future temperature at each sampling site minus either the mean or maximum temperature within their contemporary genomic province.** For most of the sites and across size fractions the future temperature projected by the bias adjusted ESM ensemble model is higher than both the maximum and mean contemporary temperature of their genomic province.

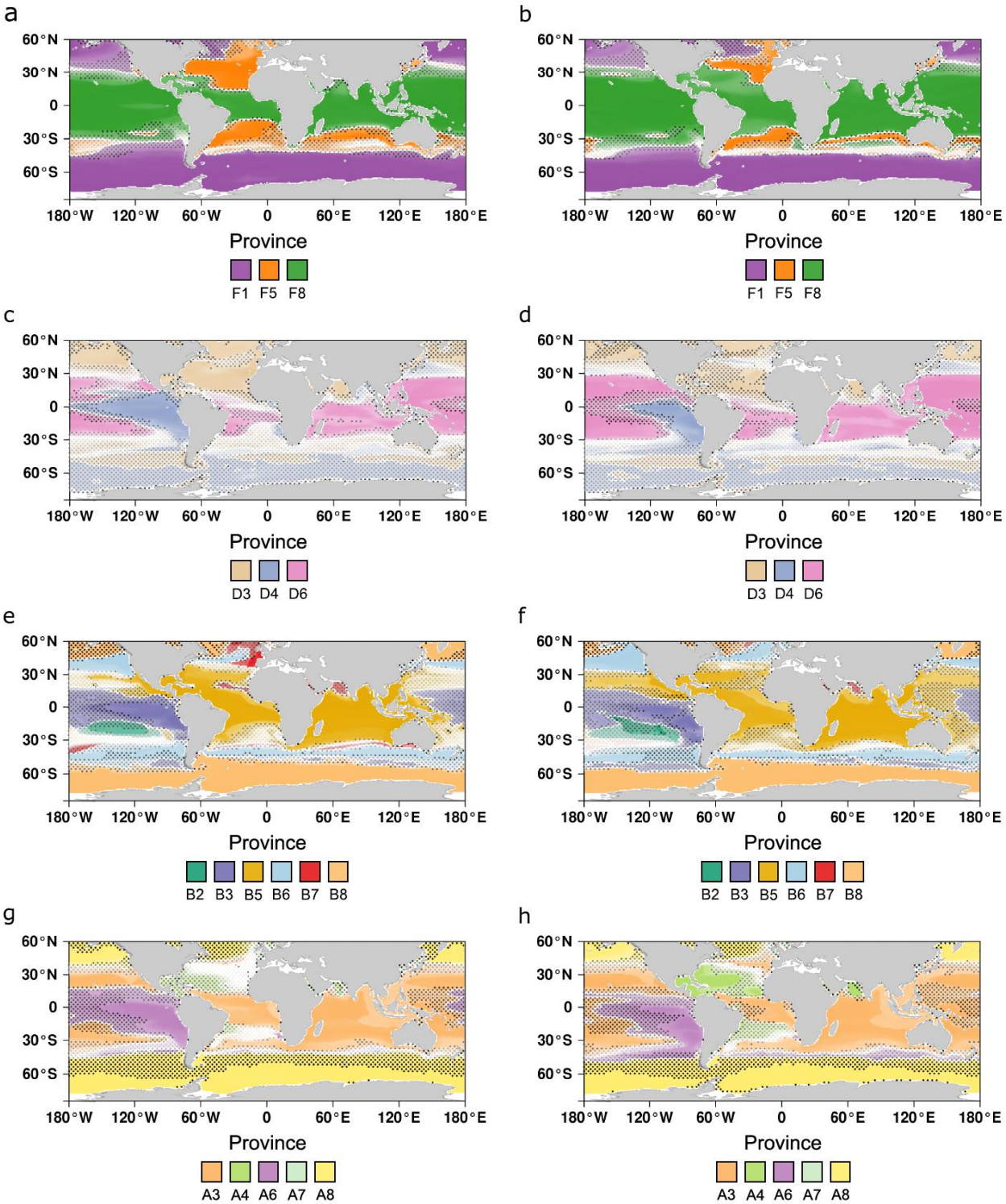


**Supplementary Fig. 14 | Global geographical patterns for 180-2000, 5-20, 0.22-3, 0-0.2 µm plankton size fractions in present day (a, c, e , g) and at the end of the century (b, d, f, h).** The dominant province *i.e.* the one predicted to have the highest probability of presence is represented at each grid point of the map. The color transparency is the probability of presence

1048 of the dominant province. Expansion of tropical provinces and shrinkage of temperate
1049 communities is consistently projected in all size fractions.

1050

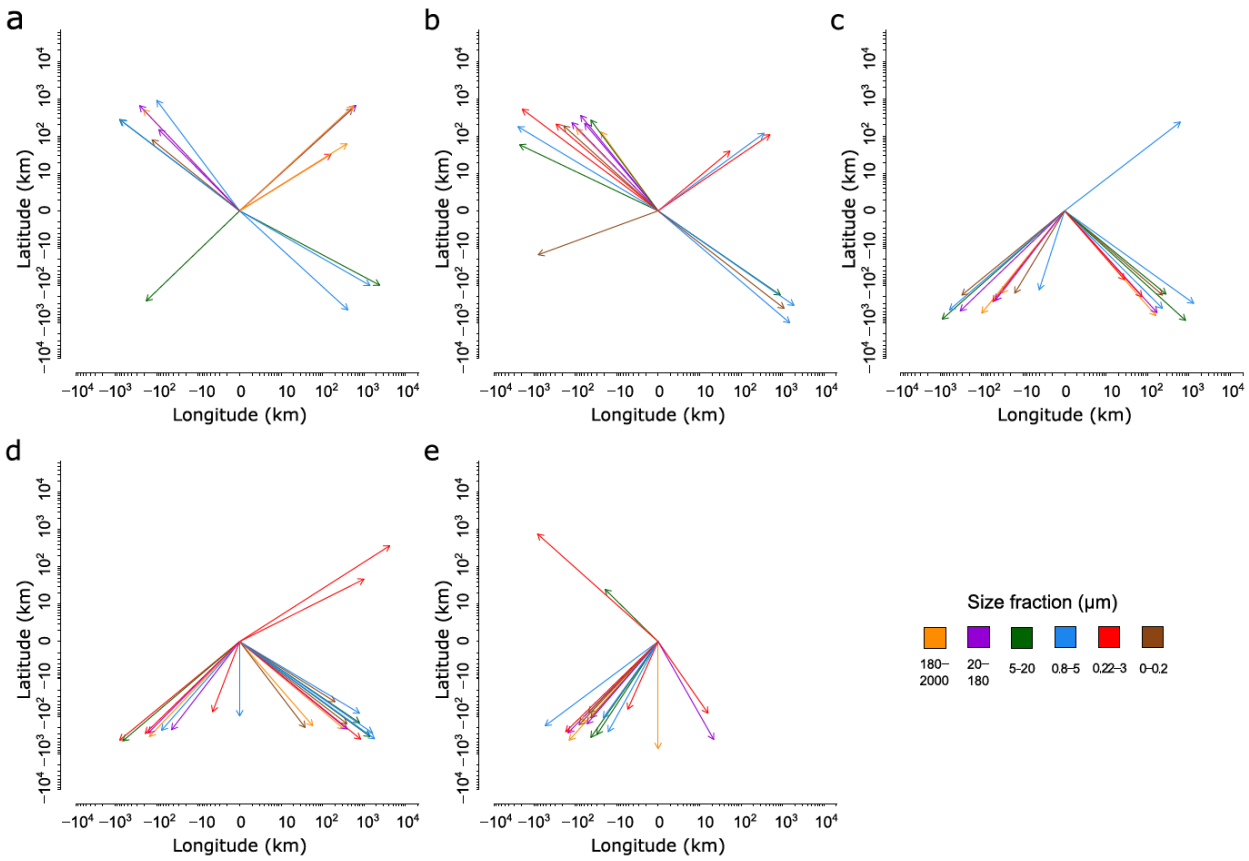


**Supplementary Fig. 15 | Projected migration shifts of the 27 provinces between present day and end of the century.** Predicted migration shifts are presented in 5 major ocean basins: (**a**) North Atlantic (**b**) North Pacific (**c**) South Atlantic (**d**) South Pacific and (**e**) Indian Ocean. 96% of migration shifts (larger than 200 km) are oriented towards the pole. Mean shift is 641 km (76 ± 79 km.dec$^{-1}$) and median shift is 394 km (47 km.dec$^{-1}$). Few provinces are projected to shift more than thousands of kilometers towards suitable environmental conditions with a maximum shift of 4325 km.

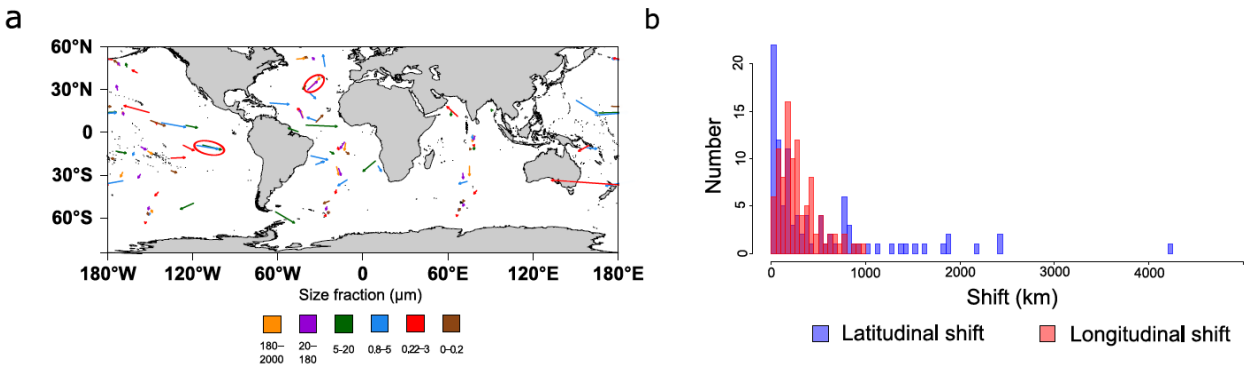


**Supplementary Fig. 16 | (a) Projected migration shifts of provinces on the world map. (b) Latitudinal shift distribution (red bars) and longitudinal shift distribution (blue bars).** (**a**) Migration shifts are represented as arrows pointing at the end of century centroid. Arrows are colored according to the size fraction. Some shifts seem to correlate with each other (exemplified with circled arrows). For instance, parallel shifts are projected in the southern pacific equatorial communities of size fractions 0.8-5 µm and 5-20 µm (blue and green circled arrows). All non-poleward arrows belong to small size classes (<20µm) showing differential responses to climate change depending on the size class. (**b**) Some longitudinal shifts are more important than latitudinal shifts with 14 longitudinal shifts superior to 1000 kms. Mean longitudinal shift (around 500 kms) is significantly higher (Student t-test[25] p-value<0.01) than mean latitudinal shift (around 290 kms) while medians (longitudinal 190 kms vs latitudinal 230 kms) are not significantly different (Wilcoxon test). The median migration speed is 47 km.dec$^{-1}$, (latitudinally 23 km.dec$^{-1}$, longitudinally 27 km.dec$^{-1}$).

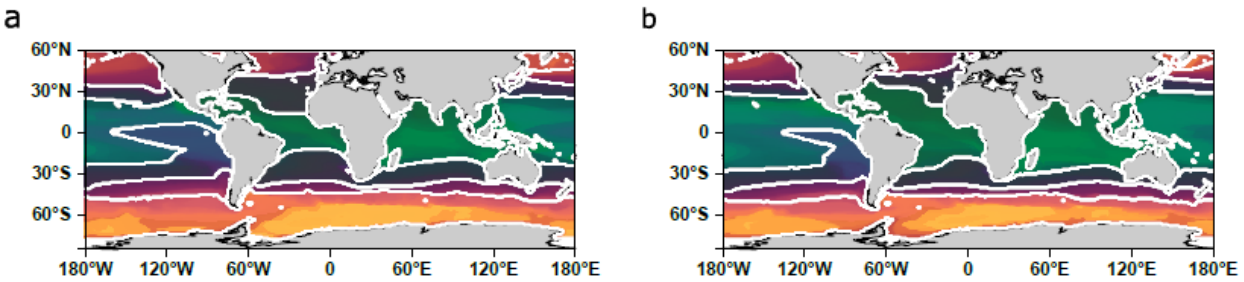


**Supplementary Fig. 17 | (a) Present day and (b) end of century combined size class biogeographies using the PHATE algorithm[7].** Each grid point is associated with a color depending on its PHATE coordinates (using three axes). Each coordinate is respectively assigned to a given degree of color between 0 and 255 according to equation 2 (either red green or blue depending on the axis). Boundaries of clusters using k-medoïds (k=4) are represented in white.

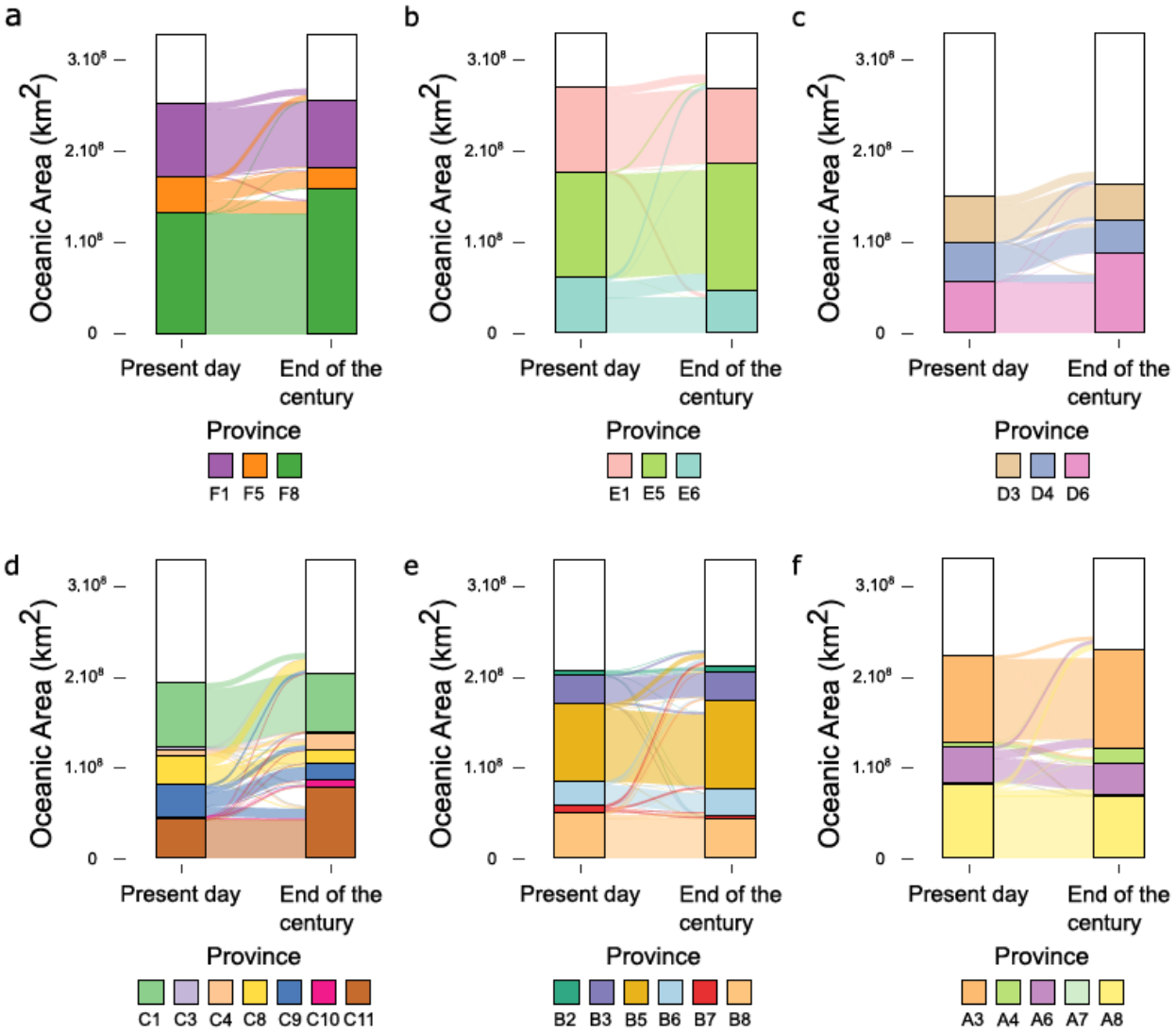


1079 **Supplementary Fig. 18 | Probabilistic covered areas of the provinces projected in present**
1080 **day and at the end of the century.** (**a**) 180-2000 µm (**b**) 20-180 µm (**c**) 5-20 µm (**d**) 0.8-5 µm
1081 (**e**) 0.22-3 µm (**f**) 0-0.2 µm. The area covered by a province is defined as the area in which this
1082 province is dominant and weighted by its probability of presence at each point and grid cell
1083 area. Areas not covered by the provinces are represented in white.
1084

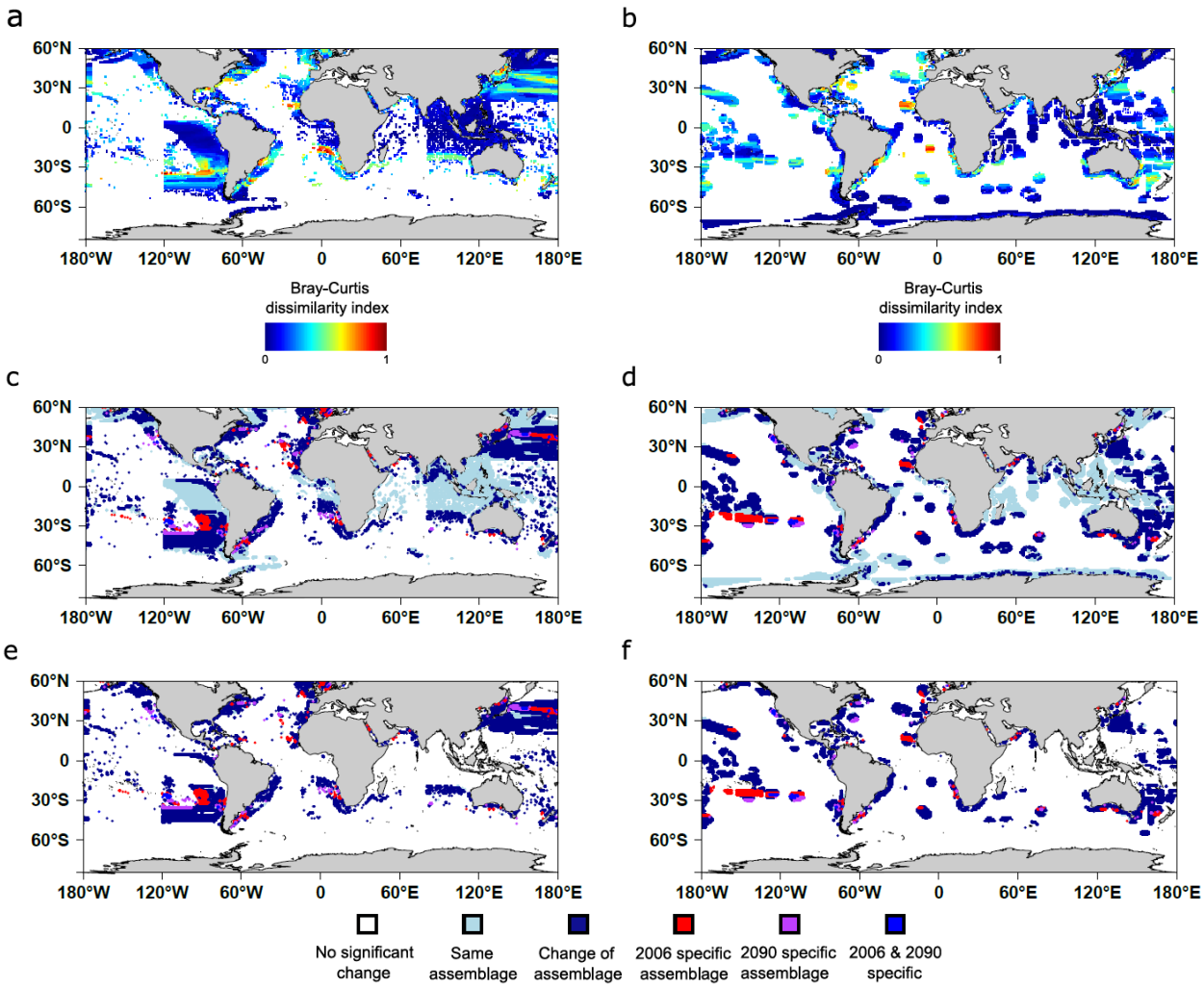


**Supplementary Fig. 19 | Bray-Curtis dissimilarity index and assemblage change maps comparing present day with end of the century projections of *dominant* provinces in (a, c, e) principal fisheries (4 last deciles[26]) and (b, d, f) Exclusive Economic Zones[27].** Assemblage changes in (**c**) Principal fisheries (**d**) Exclusive Economic Zones. Assemblage changes in (**e**) Principal fisheries (**f**) Exclusive Economic Zones with a Bray-Curtis dissimilarity index superior to 1/6.

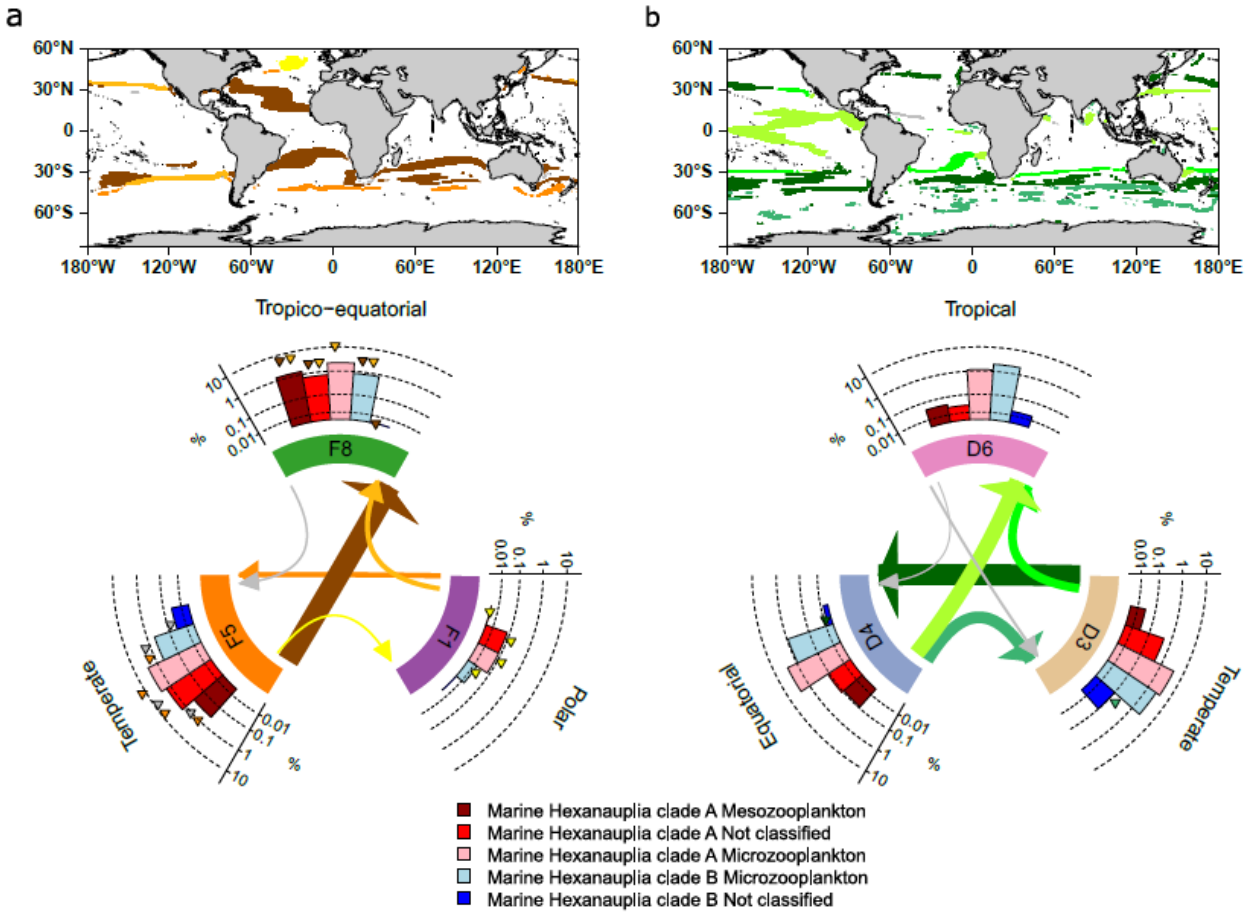


**Supplementary Fig. 20 | Projected compositional change in marine hexanauplia in areas of dominant community change in the five major basins in size fraction (a) 180-2000 µm and (b) 5-20 µm.** Top: Areas of dominant community change are highlighted using different colors depending on the dominant community transition. Bottom: Circular plots summarizing significant compositional shifts in marine hexanauplia: each type of transition is colored differently and according to the one on the map or in grey if they represent less than 2% of the transitions. Barplots represent mean relative abundances in 5 types of Marine Hexanauplia (copepods) based on genome abundance[28] in the given province. Arrows represent dominant community shifts pointing towards the end of the century projected province and their widths are proportional to the area of change. Significant compositional changes in a type of genome (*e.g.* mesozooplankton from clade A) are represented by triangles of the associated transition color above the corresponding bar (*e.g.* dark red for mesozooplankton from clade A) of the barplot of the province projected at the end of the century (which is at the tip of the arrow).

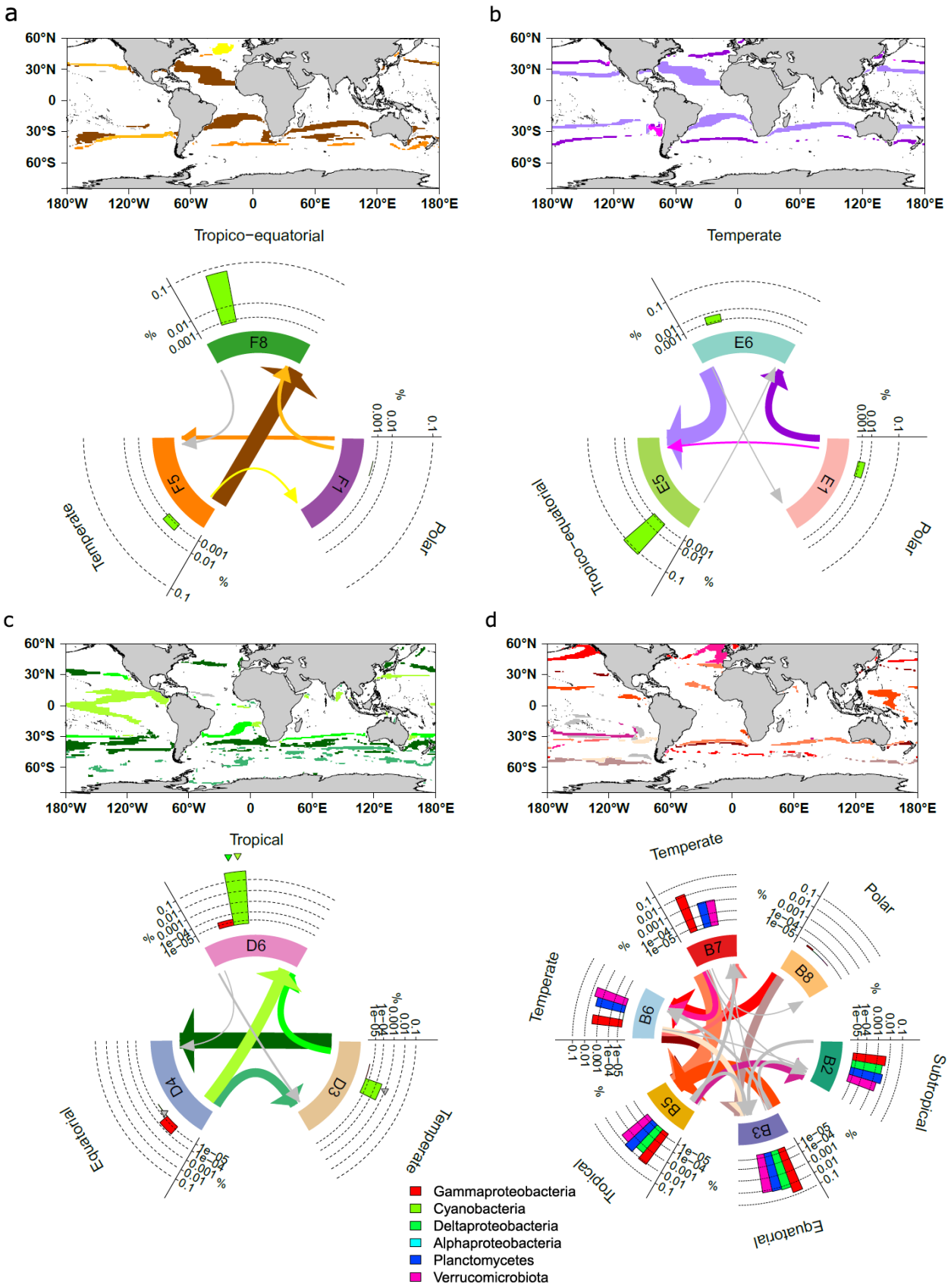


**Supplementary Fig. 21 | Projected compositional change in bacterial diazotrophs**

**in areas of dominant community change in the five major basins in size fraction (a) 180-2000 µm (b) 20-180 µm (c) 5-20 µm and (d) 0.22-3 µm.** Top: Areas of dominant community change are highlighted using different colors depending on the dominant community transition. Bottom: Circular plots summarizing significant compositional shifts in marine diazotrophs: each type of transition is colored differently and according to the one on the map or in grey if they represent less than 2% of the transitions. Barplots represent mean relative abundances in main clades of marine diazotrophs[22] based on genome abundance in the given province. Arrows represent dominant community shifts pointing towards the end of the century projected province and their widths are proportional to the area of change. Significant compositional changes in a type of genome (*e.g.* cyanobacteria) are represented by triangles of the associated transition color above the corresponding bar (*e.g.* yellowgreen for cyanobacteria) of the barplot of the province projected at the end of the century (which is at the tip of the arrow).

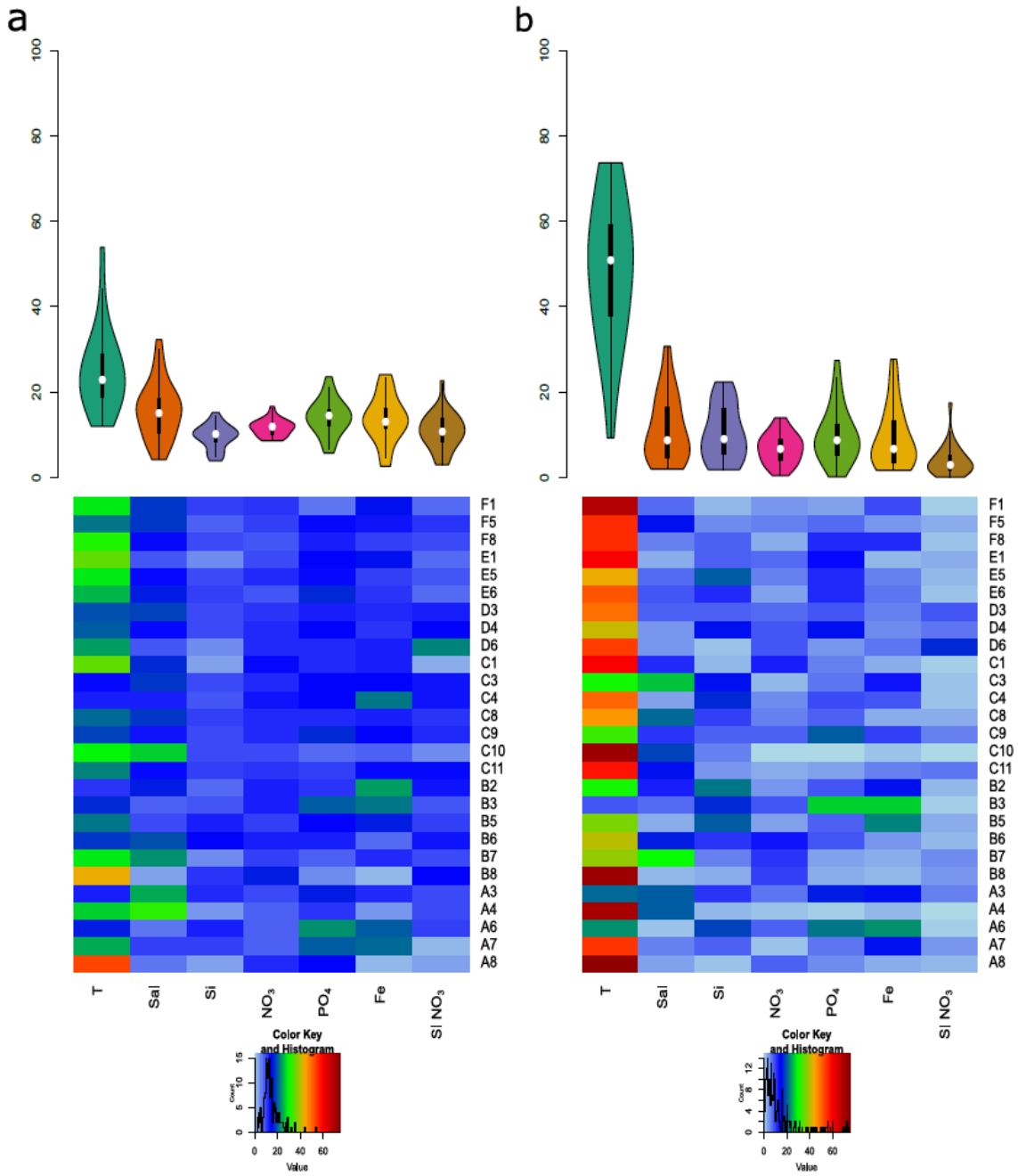


**Supplementary Fig. 22 | Distributions and heat maps of the relative influences of the different drivers in (a) defining single niches associated with the provinces from DALEX R package[29] (b) driving climate change associated reorganization of single provinces.** Median relative influence of Temperature is significantly higher than for all other environmental parameters (Pairwise Wilcoxon test p<0.01 for all parameters) in (**a**) defining the niches and (**b**) driving province reorganization**.** This is also the case within individual size fractions for (**b**) but not for (**a**). Respectively, Salinity (Sal) and Phosphate ($PO_4$), have second and third highest median relative influences far behind Temperature whereas dissolved Silica and seasonality

1130 index of Nitrate (SI $NO_3$) have the lowest median relative importance in (**a**)**.** Numbers above
1131 violins are median (and mean) relative influences.
1132

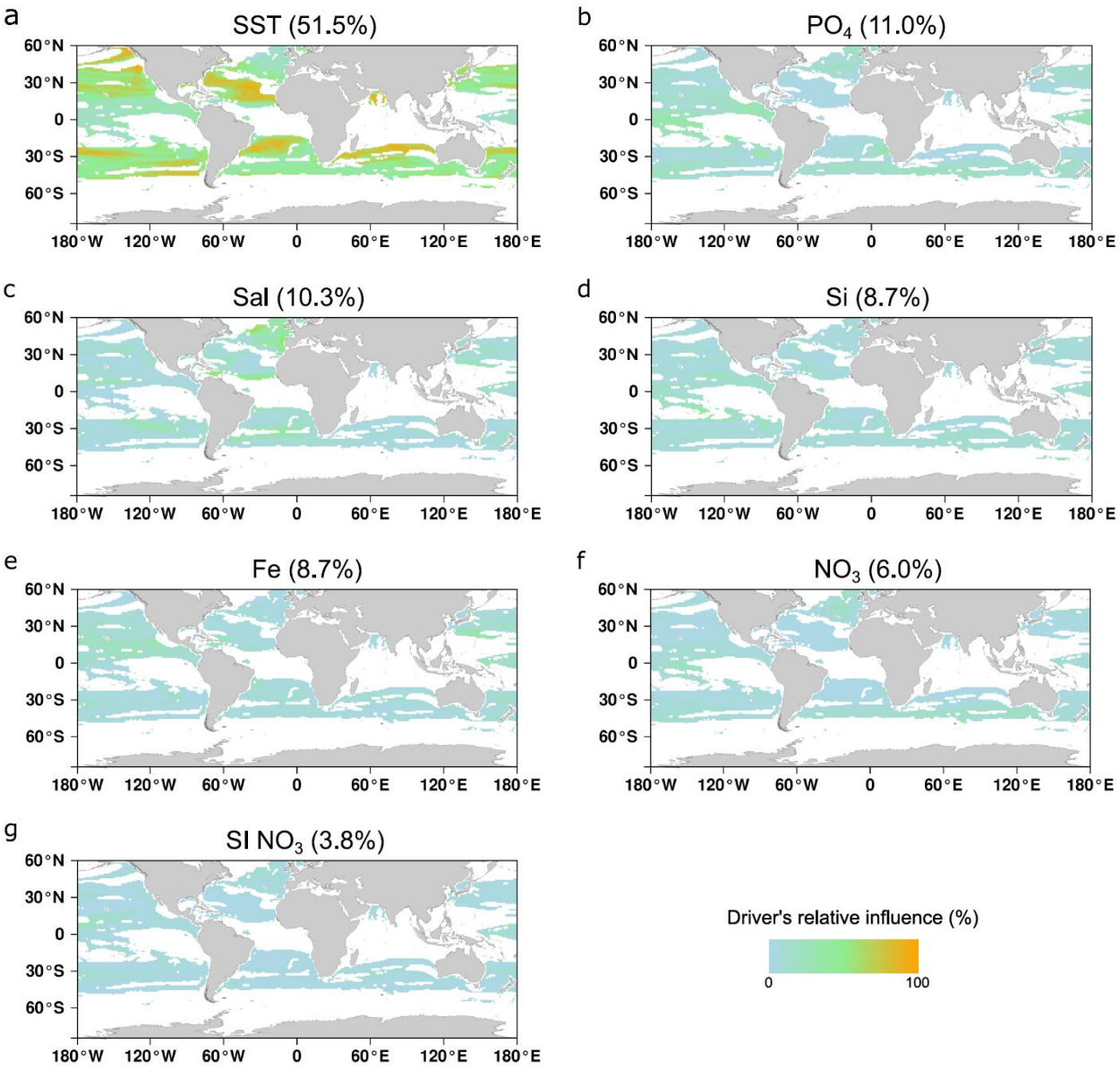


**Supplementary Fig. 23 | Maps of environmental drivers' relative influences in driving province reorganization.** Each environmental parameter's relative influence is quantified by considering only the variation of each parameter individually between present day and end of the century as defined in Barton et al.[30] (*Materials and Methods*) and where a significant change is projected. Importantly the mean impact of SST (51.5%) is to a great extent the highest. $PO_4$ is the second most impacting driver (11.0%). Contrary to supplementary Fig. 24, relative influence is calculated here by combining all provinces together. Therefore, mean relative influences slightly differ especially for dissolved silica (Si).

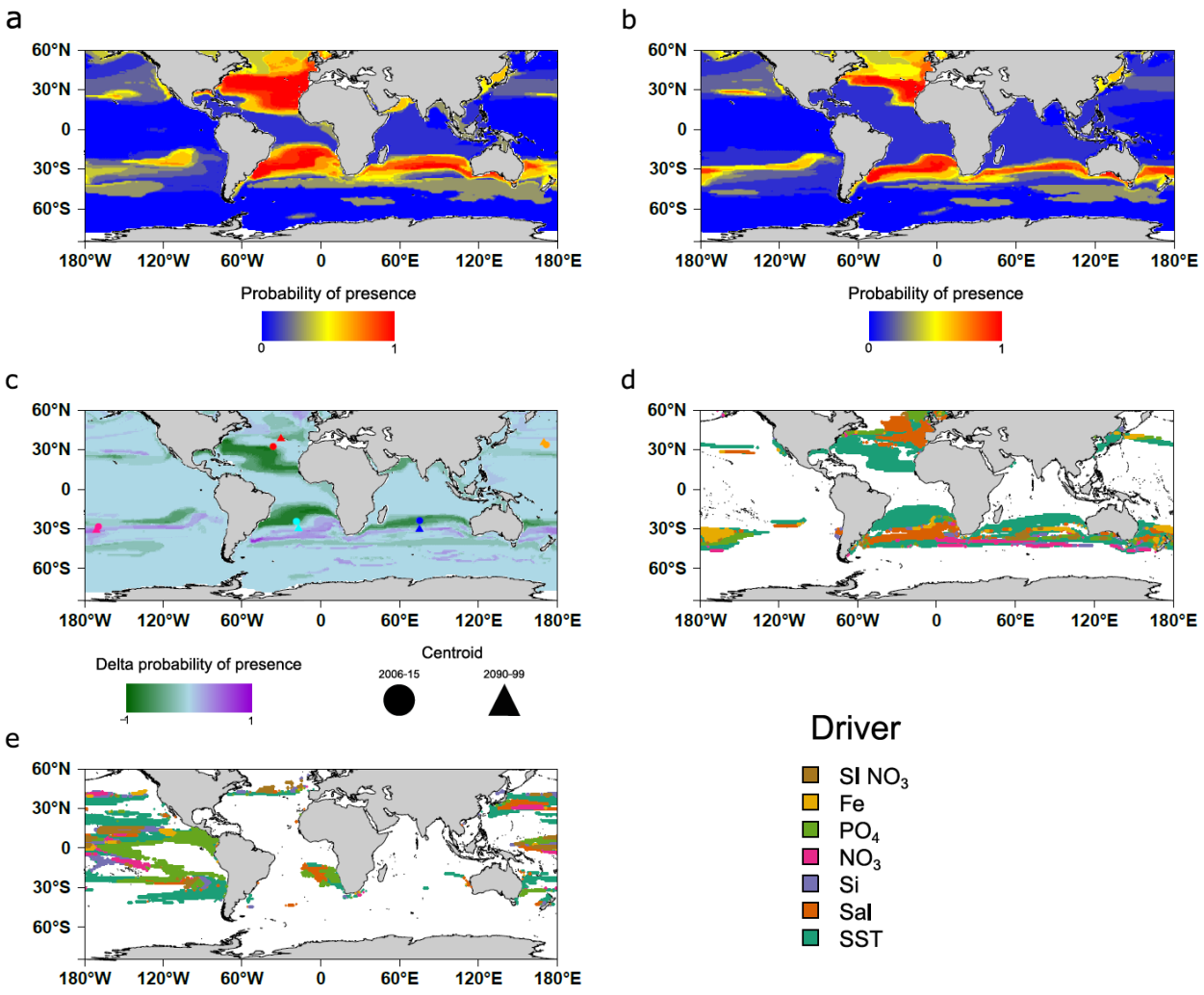


**Supplementary Fig. 24 | Projection maps of province F5 of size fraction 180-2000 µm in present day (a), at the end of the century (b) and their difference (c); Drivers of changes for province F5 (d) and C9 (e).** At each grid point, the probability of presence of the province is computed as the average of the predicted probability of each of the four machine learning techniques (gbm, nn, rf and gam). Red color indicates a high probability of presence. (**a**)The projected province corresponds to the sampled province (North Atlantic and South Atlantic) but several other places have high probabilities of presence such as South Australia where no sampling is available. (**b**) At the end of the century, the province is projected to reduce significantly in size. (**c**) Delta probability of presence map (2006/15 – 2090/99) and core range shift in the 5 major oceanic basins of province F5 of size fraction 180-2000 µm. In all the basins, the centroid of the province is projected to migrate poleward. (**d**) Main drivers associated with the projected changes. Changes are mainly driven by sea surface temperature (56%) followed by salinity (16%). (**e**) Main drivers associated with the shrinkage of the equatorial cluster C9 of

size fraction 0.8-5. Considering only latitudes between the two tropics, changes are mainly driven by decreases in $PO_4$ (24%) in addition to SST (27%) (overall 34% STT and 20% $PO_4$).

| Model | Reference |
|---|---|
| CESM1-BGC | Gent et al., 2011[13] |
| GFDL-ESM2G | Dunne et al., 2013[14] |
| GFDL-ESM2M | Dunne et al., 2013[14] |
| HadGEM2-ES | Collins et al., 2011[15] |
| IPSL-CM5A-LR | Dufresne et al., 2013[16] |
| IPSL-CM5A-MR | Dufresne et al., 2013[16] |
| MPI-ESM-LR | Giorgetta et al., 2013[17] |
| MPI-ESM-MR | Giorgetta et al., 2013[17] |
| NorESM1-ME | Bentsen et al., 2013[18] |

**Supplementary Table 1 | Earth System models used to compute the mean model.**

1162

| Fraction | Province | Climatic annotation | Area 2006-15 ($MKm^2$) | Area 2090-99 ($MKm^2$) | Delta area ($MKm^2$ (%)) |
|---|---|---|---|---|---|
| 180-2000 | F1 | polar | 82 | 73 | -9 (-11%) |
| 180-2000 | F5 | temperate | 44 | 26 | -18 (-41%) |
| 180-2000 | F8 | tropico-equatorial | 140 | 169 | +29 (+21%) |
| 20-180 | E1 | polar | 97 | 84 | -13 (-13%) |
| 20-180 | E5 | tropico-equatorial | 119 | 145 | +26 (+22%) |
| 20-180 | E6 | temperate | 65 | 49 | -15 (-23%) |
| 5-20 | D3 | temperate | 51 | 41 | -10 (-20%) |
| 5-20 | D4 | equatorial | 46 | 37 | -8 (-18%) |
| 5-20 | D6 | tropical | 65 | 97 | +32 (+48%) |
| 0.8-5 | C1 | polar | 71 | 64 | -6 (-8%) |
| 0.8-5 | C3 | subtropical | 3,6 | 1,4 | -2,2 (-61%) |
| 0.8-5 | C4 | subtropical | 6 | 19 | +13 (+217%) |
| 0.8-5 | C8 | temperate | 33 | 15 | -18 (-54%) |
| 0.8-5 | C9 | equatorial | 35 | 19 | -16 (-45%) |
| 0.8-5 | C10 | subtropical | 3.8 | 7.4 | +3,6 (+95%) |
| 0.8-5 | C11 | tropical | 49 | 86 | +37 (+75%) |
| 0.22-3 | B2 | subtropical | 5,1 | 6,7 | +1,6 (+31%) |
| 0.22-3 | B3 | equatorial | 33 | 32 | -1 (-0.3%) |
| 0.22-3 | B5 | tropical | 88 | 102 | +13 (+15%) |
| 0.22-3 | B6 | temperate | 30 | 35 | +5 (+17%) |
| 0.22-3 | B7 | temperate | 8 | 2 | -6 (-75%) |
| 0.22-3 | B8 | polar | 51 | 44 | -7 (-14%) |
| 0-0.2 | A3 | tropical | 101 | 114 | +13 (+13%) |
| 0-0.2 | A4 | subtropical | 6 | 19 | +13 (+216%) |
| 0-0.2 | A6 | equatorial | 40 | 36 | -4 (-10%) |
| 0-0.2 | A7 | temperate | 1,7 | 1 | -0,7 (-41%) |
| 0-0.2 | A8 | polar | 81 | 67 | -14 (-17%) |

1163 **Supplementary Table 2 | Genomic provinces climatic annotations and oceanic surfaces**
1164 **covered in present day (2006-15) and at the end of the century (2090-990).**

1165

| | Fraction (µm) | SST | Sal | Si | NO3 | PO4 | Fe | SI NO3 |
|---|---|---|---|---|---|---|---|---|
| Niche definition | 180-2000 | 27,7 | 16,8 | 10,1 | 10,3 | 11,4 | 14 | 9,7 |
| | 20-180 | 29,7 | 13,3 | 8,9 | 10,7 | 16,3 | 13,2 | 7,9 |
| | 5-20 | 21,5 | 14,2 | 8,4 | 12,7 | 13,7 | 12,6 | 17 |
| | 0,8-5 | 22,6 | 17,3 | 9,2 | 12,3 | 13,4 | 14,5 | 10,8 |
| | 0,22-3 | 23,9 | 13,7 | 10,5 | 13 | 12,5 | 14,2 | 12,2 |
| | 0-0,2 | 27,1 | 16,4 | 9,3 | 9,5 | 17,9 | 12,1 | 7,6 |
| | all | 25 | 15,5 | 9,5 | 11,6 | 14,2 | 13,6 | 10,8 |
| Climate change | 180-2000 | 75,2 | 8,4 | 2,5 | 2,6 | 4,1 | 5,8 | 1,4 |
| | 20-180 | 71,7 | 4,2 | 7,3 | 3,9 | 8,7 | 3,3 | 1,0 |
| | 5-20 | 57,9 | 6,1 | 4,4 | 6,6 | 9,0 | 6,5 | 1,0 |
| | 0,8-5 | 54,9 | 13,4 | 7,2 | 5,5 | 9,7 | 5,9 | 3,6 |
| | 0,22-3 | 42,6 | 9,9 | 13,5 | 6,4 | 9,1 | 15,2 | 3,3 |
| | 0-0,2 | 42,3 | 18,9 | 6,6 | 6,4 | 12,1 | 10,8 | 2,9 |
| | all | 51,5 | 10,3 | 8,7 | 6 | 11 | 8,7 | 3,8 |

**Supplementary Table 3 | Summary table of the relative importance of each environmental driver in niche definition and in driving geographical reorganization in response to climate change.** Note that in both cases (niche definition and climate change), the row 'all' is not the mean over the size fractions. In the case of niche definition, this is due to a different number of niches in each size class. In the case of climate change, relative influence is either calculated for single provinces at a given grid point then recalculated for individual size class or calculated for all provinces together (row 'all').

## References

1. Ridgeway, G. gbm: Generalized Boosted Regression Models. *R Packag. version 1.6-3.1* (2010).

2. Breiman, L. & Cutler, A. Breiman and Cutler's random forests for classification and regression. *Packag. 'randomForest'* (2012). doi:10.5244/C.22.54

3. Venables, W. N. & Ripley, B. D. *Modern Applied Statistics with S Fourth edition by*. *World* (2002). doi:10.2307/2685660

4. Wood, S. N. Stable and efficient multiple smoothing parameter estimation for generalized additive models. *J. Am. Stat. Assoc.* (2004). doi:10.1198/016214504000000980

5. Wilcoxon, F. Individual Comparisons by Ranking Methods. *Biometrics Bull.* **1**, (1945).

6. Jones, M. C. & Cheung, W. W. L. Multi-model ensemble projections of climate change effects on global marine biodiversity. *ICES J. Mar. Sci.* (2015). doi:10.1093/icesjms/fsu172

7. Moon, K. R. *et al.* Visualizing Structure and Transitions for Biological Data Exploration. *SSRN Electron. J.* (2018). doi:10.2139/ssrn.3155891

8. Orsi, A. H., Whitworth, T. & Nowlin, W. D. On the meridional extent and fronts of the Antarctic Circumpolar Current. *Deep. Res. Part I* (1995). doi:10.1016/0967-0637(95)00021-W

9. Longhurst, A. R. *Ecological Geography of the Sea*. *Ecological Geography of the Sea* (2007). doi:10.1016/B978-0-12-455521-1.X5000-1

10. Reygondeau, G. *et al.* Dynamic biogeochemical provinces in the global ocean. *Global Biogeochem. Cycles* (2013). doi:10.1002/gbc.20089

11. Fay, A. R. & McKinley, G. A. Global open-ocean biomes: Mean and temporal variability. *Earth Syst. Sci. Data* (2014). doi:10.5194/essd-6-273-2014

12. Boyer, T. P. *et al.* WORLD OCEAN DATABASE 2013, NOAA Atlas NESDIS 72. *Sydney Levitus, Ed.; Alexey Mishonoc, Tech. Ed.* (2013). doi:10.7289/V5NZ85MT

13. Gent, P. R. *et al.* The community climate system model version 4. *J. Clim.* (2011). doi:10.1175/2011JCLI4083.1

14. Dunne, J. P. *et al.* GFDL's ESM2 global coupled climate-carbon earth system models.

Part II: Carbon system formulation and baseline simulation characteristics. *J. Clim.* (2013). doi:10.1175/JCLI-D-12-00150.1

15. Collins, W. J. *et al.* Development and evaluation of an Earth-System model - HadGEM2. *Geosci. Model Dev.* (2011). doi:10.5194/gmd-4-1051-2011

16. Dufresne, J. L. *et al.* Climate change projections using the IPSL-CM5 Earth System Model: From CMIP3 to CMIP5. *Clim. Dyn.* (2013). doi:10.1007/s00382-012-1636-1

17. Giorgetta, M. A. *et al.* Climate and carbon cycle changes from 1850 to 2100 in MPI-ESM simulations for the Coupled Model Intercomparison Project phase 5. *J. Adv. Model. Earth Syst.* (2013). doi:10.1002/jame.20038

18. Bentsen, M. *et al.* The Norwegian Earth System Model, NorESM1-M – Part 1: Description and basic evaluation of the physical climate. *Geosci. Model Dev.* (2013). doi:10.5194/gmd-6-687-2013

19. van Vuuren, D. P. *et al.* The representative concentration pathways: An overview. *Clim. Change* (2011). doi:10.1007/s10584-011-0148-z

20. Fawcett, T. An introduction to ROC analysis. *Pattern Recognit. Lett.* (2006). doi:10.1016/j.patrec.2005.10.010

21. Jaccard, P. Distribution comparée de la flore alpine dans quelques régions des Alpes occidentales et orientales. *Bull. la Murithienne* (1902).

22. Delmont, T. O. *et al.* Heterotrophic bacterial diazotrophs are more abundant than their cyanobacterial counterparts in metagenomes covering most of the sunlit ocean. *bioRxiv* 2021.03.24.436778 (2021). doi:10.1101/2021.03.24.436778

23. Aumont, O., Ethé, C., Tagliabue, A., Bopp, L. & Gehlen, M. PISCES-v2: An ocean biogeochemical model for carbon and ecosystem studies. *Geosci. Model Dev.* (2015). doi:10.5194/gmd-8-2465-2015

24. Michelangeli, P. A., Vrac, M. & Loukos, H. Probabilistic downscaling approaches: Application to wind cumulative distribution functions. *Geophys. Res. Lett.* (2009). doi:10.1029/2009GL038401

25. The probable error of a mean. *Biometrika* **6**, (1908).

26. Watson, R. A. A database of global marine commercial, small-scale, illegal and unreported fisheries catch 1950-2014. *Sci. Data* (2017). doi:10.1038/sdata.2017.39

1234 27. Flanders Marine Institute (2018). Maritime Boundaries Geodatabase: Maritime
1235 Boundaries and Exclusive Economic Zones (200NM), version 10. (2018).
1236 doi:https://doi.org/10.14284/313.

1237 28. Delmont, T. O. *et al.* Functional repertoire convergence of distantly related eukaryotic
1238 plankton lineages revealed by genome-resolved metagenomics. *bioRxiv*
1239 2020.10.15.341214 (2020). doi:10.1101/2020.10.15.341214

1240 29. Biecek, P. DALEX: explainers for complex predictive models. *J. Mach. Learn. Res.* **19**, 1–
1241 5 (2018).

1242 30. Barton, A. D., Irwin, A. J., Finkel, Z. V. & Stock, C. A. Anthropogenic climate change
1243 drives shift and shuffle in North Atlantic phytoplankton communities. *Proc. Natl. Acad.*
1244 *Sci.* (2016). doi:10.1073/pnas.1519080113